Measurement Science and Technology

100 year anniversary
Measurement Science and Technology

PAPER • **OPEN ACCESS**

The pioneer of intelligent and sustainable construction in tunnel shotcrete applications: a comprehensive experimental and numerical study on a self-sensing and self-heating green cement-based composite

To cite this article: Mohammadmahdi Abedi *et al* 2024 *Meas. Sci. Technol.* **35** 065601

OPEN ACCESS
IOP Publishing
Measurement Science and Technology
Meas. Sci. Technol. **35** (2024) 065601 (28pp)
https://doi.org/10.1088/1361-6501/ad338e

The pioneer of intelligent and sustainable construction in tunnel shotcrete applications: a comprehensive experimental and numerical study on a self-sensing and self-heating green cement-based composite

Mohammadmahdi Abedi[1,*], Federico Gulisano[2], Baoguo Han[3], Raul Fangueiro[4] and António Gomes Correia[1]

[1] Department of Civil Engineering, University of Minho, ISISE, ARISE, Campus de Azurém, 4800-058 Guimarães, Portugal
[2] Departamento de Ingeniería del Transporte, Territorio y Urbanismo, Universidad Politécnica de Madrid, C/Profesor Aranguren 3, 28040 Madrid, Spain
[3] School of Civil Engineering, Dalian University of Technology, Dalian 116024, People's Republic of China
[4] Department of Textile Engineering, Centre for Textile Science and Technology, University of Minho, Campus de Azurém, 4800-058 Guimarães, Portugal

E-mail: id8012@alunos.uminho.pt and mohammadmehdi.abedi@gmail.com

Received 23 January 2024, revised 27 February 2024
Accepted for publication 13 March 2024
Published 27 March 2024

Abstract
In this study, a self-sensing and self-heating natural fibre-reinforced cementitious composite for the shotcrete technique was developed using Kenaf fibres. For this purpose, a series of Kenaf fibre concentrations were subjected to initial chemical treatment, followed by integration into the cement-based composite containing hybrid carbon nanotubes (CNT) and graphene nanoplatelets (GNP). The investigation encompassed an examination of mechanical, microstructural, sensing, and joule heating performances of the environmentally friendly shotcrete mixture, with subsequent comparisons drawn against a counterpart blend featuring a conventionally synthesized polypropylene (PP) fibre. Following the experimental phase, a comprehensive 3D nonlinear finite difference (3D NLFD) model of an urban twin road tunnel, completed with all relevant components, was meticulously formulated using the FLAC3D (fast lagrangian analysis of continua in 3 dimensions) code. This model was subjected to rigorous validation procedures. The performances of this green shotcrete mixture as the lining of the inner shell of the tunnel were assessed comparatively using this 3D numerical model under static and dynamic loading. The twin tunnel was subjected to a harmonic seismic load as a

* Author to whom any correspondence should be addressed.

dynamic load with a duration of 15 s. The laboratory findings showed a reduction in the composite sensing and heating potentials in both cases of Kenaf and PP fibre reinforcement. Incorporating a specific quantity of fibre yields a substantial enhancement in both the mechanical characteristics and microstructural attributes of the composite. An analysis of digital image correlation demonstrated that Kenaf fibres were highly effective in controlling cracks in cement-based composites. Furthermore, based on the static and dynamic 3DNLFD analysis, this green cement-based composite demonstrated its potential for shotcrete applications as the lining of the inner shell of the tunnel. This study opens an appropriate perspective on the extensive and competent contribution of natural fibres for multifunctional sustainable, reliable and affordable cement-based composite developments for today's world.

Keywords: natural fibres, synthesized fibres, shotcrete lining, self-sensing, self-heating, tunnel simulation, finite difference method (FDM)

1. Introduction

Natural fibres, which are widely recognized for their biodegradability, low density, affordability, durability, and sustainable nature, possess a greater ability to absorb energy and are abundantly available in the environment [1]. The fundamental components of natural fibres, namely hemicellulose, cellulose, and lignin enjoy broad recognition in the scientific community. The mechanical characteristics of these fibres are predominantly governed by the content of cellulose and the orientation of their micro-fibrils [2, 3]. Present-day engineering advancements strive to produce high-performance engineering materials utilizing natural resources in response to the growing need for cost-effective, environmentally friendly, and sustainable construction practices. Natural fibre-reinforced composites based on cement-based materials (such as concrete, mortar, stabilized geomaterials, etc) represent a significant milestone in the ongoing research on eco-friendly materials in this century [4]. Undoubtedly, there is a rising trend towards the adoption of sustainable construction materials that effectively utilize renewable resources [5–7]. In general, the integration of fibres into cement-based composites has the potential to enhance their flexural stiffness [8], corrosion resistance [9], ductility [10], cement hydration process, and crack control [11]. The lining of tunnels depends heavily on these features. Despite the fact that synthetic fibres like steel and polypropylene continue to be extensively employed to enhance the mechanical properties of cement-based composites due to their established effectiveness, their high cost can lead to increased construction expenses and environmental pollution [12–14]. In contrast, natural fibres necessitate minimal energy input during the manufacturing process and offer a more economical, sustainable, and environmentally friendly option for improving the performance of cement-based composites in the long run [4, 15, 16]. A multitude of investigations has been undertaken to assess the performance of diverse cement-based composites incorporating various types of natural fibres, including but not limited to sisal, straw, jute, palm, and hemp among others [17, 18]. Drawing upon an extensive review of existing literature, a majority of studies offer a comprehensive assessment of the potential of natural fibres to enhance the physical and mechanical characteristics of cement-based composites [19–21]. Notably, these natural fibres have proven effective in ameliorating the post-peak behaviour of cement-based composites and in reducing brittle failure, as evidenced by several investigations [22, 23]. Among the natural fibre options, Kenaf-based fibres emerge as superior alternatives to synthetic fibres for use in cement-based composites, when compared to other varieties of natural fibres. This preference is primarily attributable to their ready availability in nature, distinctive microstructure, elevated tensile strength, and the minimal energy demands associated with their extraction and processing [24, 25]. Nevertheless, when compared to other natural fibres, Kenaf-based fibres demonstrate relatively superior physical and mechanical properties and exhibit a simpler dispersion process in cement-based composites [26, 27]. Shotcrete, also known as (trademark) Gunite, is sprayed concrete or mortar [28]. Shotcrete is unquestionably a blend of Portland cement and aggregate that is propelled through a spray gun nozzle by compressed air, with the addition of water. The resulting wet mixture is promptly sprayed onto the desired surface and can be shaped or smoothed soon after application. Shotcrete can be applied to surfaces of various types and shapes, including vertical and overhead areas. It possesses remarkable compressive strength, excellent durability, water resistance, resistance to frost, and offers a speedy and cost-effective implementation process [29]. As a modern construction technique, shotcrete is used for structural repair, landslides, slope stability, and line tunnel wall covering as well as many other construction projects [30]. In general, shotcrete can be classified as either wet-mixed or dry-mixed [29]. However, it is more desirable to use wet-mix shotcrete since this method involves less dust engulfment [29, 31]. Thus, wet-mix shotcrete is employed here since it can be controlled effectively under suitable pressure through further quality control. Compared with traditional concrete, shotcrete uses a unique application process. Fibres have been widely used for the production process of fibrous concrete mixtures in the concrete according to ACI committee reports [32].

The convergence of nanotechnology and concrete science has given rise to a groundbreaking era in construction materials, where self-sensing and self-heating capabilities are seamlessly embedded into the electrical conductive concrete matrix [5, 33–35]. Self-sensing concrete involves the incorporation of conductive fillers such as carbon nanomaterials (CNMs) and microfibres including steel and carbon fibres, forming a conductive network that can detect variations in strain, stress, or other structural parameters within the concrete [1, 13, 36–39]. This real-time monitoring capability offers unprecedented insights into the structural health of the material, enabling early detection of potential issues and facilitating timely maintenance interventions [40–45]. Simultaneously, the inclusion of conductive fillers unlocks the potential for self-heating, where controlled electrical currents can be applied to induce localized heat within the concrete matrix [46]. This feature holds promise for applications ranging from de-icing and self-healing to energy-efficient environmental control within structures [33, 34]. In light of earlier research showcasing the restricted effectiveness of electrically conductive cement pastes and mortars in structural contexts due to inherent issues like diminished strength and inadequate volume stability, there is an emerging inclination to enhance the physical characteristics of structural materials through the integration of fibre-reinforced concrete [13]. Meanwhile, prior investigations have highlighted the efficacy of hybrid carbon nanotubes (CNTs) and graphene nanoplatelets (GNPs) in lowering the percolation threshold [1, 47]. This is achieved through the amplification of tunnelling effects resulting from the synergistic combination of 1D and 2D geometrically shaped fillers, leading to an increase in aspect ratio and specific surface area. It not only assists in cost reduction but also prevents the formation of agglomerations, which may result in physical impairment [40, 48]. Based on the literature, various studies have been carried out on self-sensing and self-heating fibre-reinforced cementitious composite [1, 36, 41, 47, 49]. However, a conspicuous gap exists in the realm of comprehensive research pertaining to the self-sensing and self-heating shotcrete mixtures, with particular emphasis on the development of environmentally friendly, cost-efficient, sustainable, and practical composites tailored for infrastructure applications. In spite of this void, the integration of natural-based fibres, particularly Kenaf, into a cement-based matrix has exhibited promising outcomes in bolstering impact resistance, chiefly attributed to the bridging mechanism enacted by these hydrophilic fibres [43]. The presence of hydrophilic cellulose within Kenaf fibres also contributes significantly to the enhancement of tensile strength, toughness, and dispersibility of the shotcrete mixture. Additionally, the use of Kenaf fibres ensures a superior surface finish, as it prevents the formation of lumps and fluff. Kenaf fibres exhibit good moisture absorption properties, enhancing the hygroscopicity of the concrete when incorporated. Moreover, the interaction between Kenaf fibres and the alkali content within the shotcrete results in heightened tensile and flexural strength for the structure, concurrently diminishing the rebound of the sprayed concrete [50].

Hence in this study, a sustainable nature-based self-sensing and self-heating cement-based composite for shotcrete application was developed using hybrid CNTs/GNPs and Kenaf fibres. The mechanical, microstructural, sensing and heating performances of this green shotcrete mixture were investigated using several tests and compared with the mixture containing a common synthesis fibre of polypropylene (PP). Subsequent to the experimental work, a detailed 3DNLFD model of an urban line tunnel including all components was developed using FLAC^{3D} (fast lagrangian analysis of continua in 3 dimensions) code and validated. The static and dynamic performances of this green shotcrete mixture as the lining of the inner shell of the tunnel were assessed comparatively using this 3D numerical model.

2. An overview of methods and materials

2.1. Raw materials

In this inquiry, the formulation of the cement-based composite entailed the use of ordinary Portland cement type I (CEM I 42.5 N) in conjunction with river sand as the fine aggregate. Furthermore, the coarse aggregate employed in the composite preparation was comprised of crushed stone with a maximum size of 10 mm. The pertinent physical and chemical attributes of both cement and aggregate are presented in figure 1, tables 1 and 2.

A compilation of the physical properties of the fibres employed in this study is presented in table 3. The fibres utilized in this research were sourced from SOO Industry Co. Korea Ltd It is important to note that natural fibres typically fall into one of three categories: vegetable fibres, mineral fibres, and animal fibres. In the context of this particular investigation, only vegetable fibres, with Kenaf being a notable example, were utilized. Natural fibres, as a whole, demonstrate commendable performance in terms of chemical resistance, bond-ability, and dispersibility. They are economically viable, environmentally sustainable, and particularly well-suited for reinforcing concrete. Moreover, their three-dimensional reinforcement imparts exceptional resistance to external impacts [51], as depicted in figure 2, which showcases both Kenaf and PP fibres employed in this study.

This research utilized multilayer GNPs and multiwall CNTs provided by Graphenest and IoLiTec companies. The morphology and characteristics of these nanomaterials are illustrated in figure 3 and table 4.

The dispersion of hybrid CNT/GNP in an aqueous suspension was accomplished through the noncovalent surfactant Pluronic F-127. Moreover, to mitigate the formation of pores due to surfactant activities, tributyl phosphate (TBP, 97%) was employed as an antifoam.

2.2. Methods

2.2.1. Fibres treatment. Numerous chemical treatments, as explored in the existing body of literature, have been subjected to examination with the aim of eliminating lignin and hemicellulose from fibres. This removal process has been

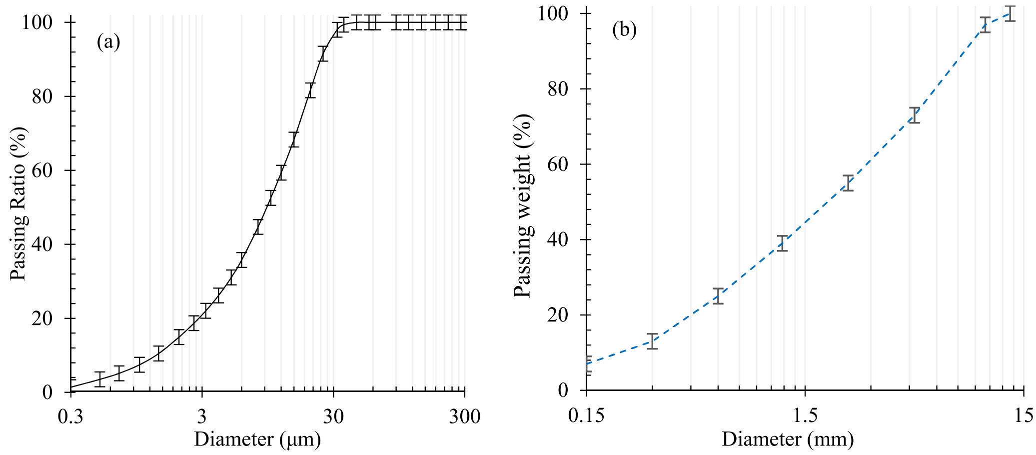

Figure 1. Particle size gradation curves of: (a) cement, (b) mixed aggregate (ASTM C136).

Table 1. Fine and coarse aggregate physical characteristics.

Type	Density (kg m^{-3})(SSD)	Fineness modulus	Absorption rate (%)	Max size
Coarse aggregate	2.62	5.46	0.93	10 mm
Fine aggregate	2.56	2.52	0.77	—

Table 2. Chemical composition and physical characteristics of ordinary Portland cement.

SiO_2 (%)	Al_2O_3 (%)	Fe_2O_3 (%)	MgO (%)	CaO (%)	Na_2O (%)	TiO_2 (%)	K_2O (%)	MnO (%)	P_2O_5 (%)	SO_3 (%)	LOI[a] (%)	Fineness, (m^2 kg^{-1})	Specific gravity (kg dm^{-3})	Initial setting time (min.)[b]	Soundness (mm) [b]
19.9	4.7	3.38	1.3	63.93	0.17	0.245	0.446	0.079	0.063	2.54	2.97	360	3.15	194	1.1

[a] (Loss on ignition) EN 196-2, [b] EN 196-3.

Table 3. The physical properties of PP, and Kenaf fibres.

Fibres	Length (mm)	Young's modulus (GPa)	Tensile strength (MPa)	Density (g cm3)	M[a] (%)	Elongation (%)	Cellulose (%)	Hemicellulose (%)	Lignin (%)	D (mm)
Kenaf	11 ± 1.0	36 ± 10	814 ± 110	1.1 ± 0.1	9.0–11.0	3.5 ± 1.0	70 ± 10	28 ± 6	15 ± 4	0.03 ± 0.01
PP	11 ± 1.0	5.2 ± 1.0	750 ± 70	0.945	0.03	15.2 ± 7	—	—	—	0.02 ± 0.01

[a] Moisture Content.

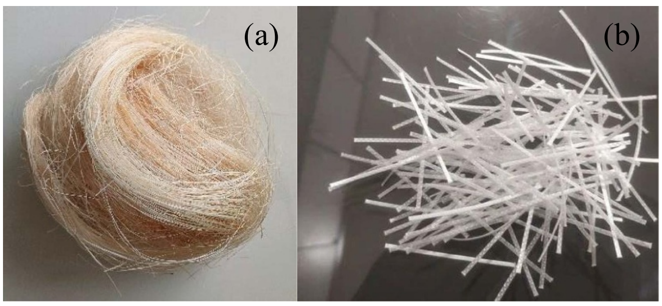

Figure 2. Fibres used in this study: (a) Kenaf fibres, (b) PP fibres.

demonstrated to extend the durability of cement-based composites reinforced with fibres. The chemical treatment alters the hydroxyl groups of the fibres and introduces additional interacting groups that facilitate effective bonding with the cement hydration products at the interface, while maintaining their environmentally friendly properties [52]. In alignment with these findings, the Kenaf fibres in this study underwent treatment employing a sodium hydroxide solution (NaOH,

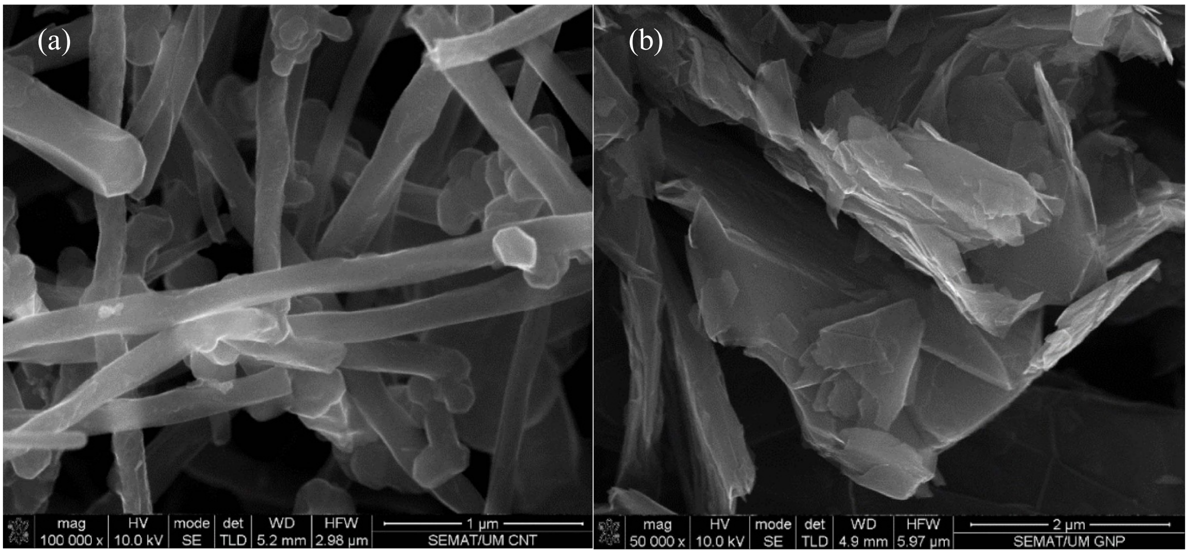

Figure 3. The structural features of carbon nanomaterials: (a) CNTs, (b) GNPs.

Table 4. The key attributes of the GNP and MWCNT utilized in this study.

GNP

Surface area (m^2 g^{-1})	Density (g cm^{-3})	Content of carbon (%)	Tensile modulus (Gpa)	PH Value (30 °C)	Tensile strength (GPa)	Layers	Dimension		Form
120–150	2.25	>99.5	1000	7–7.65	5	<20	Thickness 4–20 nm	Diameter 5–10 µm	Gray powder

MWCNT

Surface area (m^2 g^{-1})	Density (g cm^{-3})	Colour	Outside diameter (nm)	Length (µm)	Ash (wt% by total weight)	Carbon content (%)
⩾380	2.17	Black	1–2	5–30	<1.5	>90

97% purity) [53, 54]. The Kenaf fibres were immersed in a NaOH solution for 24 h at room temperature, the optimal duration for surface modification [55]. After completing the treatment, the fibres were extracted, washed thrice with tap water to eliminate residual sodium hydroxide, and air-dried at room temperature for 48 h. Subsequently, a post-drying process was also performed in an oven at a constant temperature of 100 °C for 6 h.

2.2.2. Carbon nanomaterials dispersion. To maintain the unique properties of carbon nanomaterials within a composite, a recently developed dispersion method [48], using TBP and Pluronic F-127, and sonication, was employed in this study. The optimal concentration for a hybrid CNT/GNP blend (1:1 ratio) in an intelligent cement-based composite was found to be approximately 1.0%. Consequently, 1.0% of hybrid CNT/GNP (1:1 ratio, relative to the weight of the cement) was employed in this study. In this method, TBP was initially dissolved in water required for the concrete mixing plan (238 Kg m^{-3}), followed by the introduction of a 10% proportion of Pluronic F-127 (relative to the weight of CNMs) into the suspension. Continuous stirring using a magnetic stirrer, followed by a 3 h bath sonication process at 40 °C, ensured effective dispersion with minimal structural damage to CNMs. Refer to figure 4 and [48] for more details.

2.2.3. Cement-based composite preparation. In accordance with the road construction shotcrete standards, the specimens in this investigation were meticulously prepared with adherence to specific parameters, including a fixed water-cement ratio of 44%, a fine aggregate ratio of 65%, and a unit binder weight of 480 kg m^{-3}. To ensure the complete saturation of dry aggregates with water, a mixing duration of five minutes was employed in the shotcrete mixer. The desired slump range was set at 120 ± 20 mm, while the target air volume was established at 6% ± 2%. Attaining the prescribed slump and air volume levels was achieved through the incorporation of a water-reducing agent and an air-entraining agent during the mixing process. Notably, the nomenclature of the specimens was derived from the type and concentration of fibres integrated into them. The specific mixed proportions of the experimental specimens designed for this study are presented in table 5.

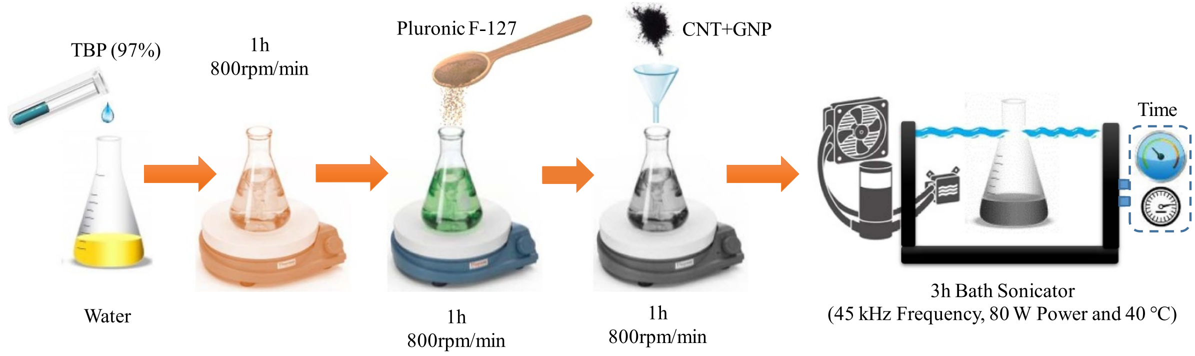

Figure 4. Dispersion methodology for CNMs employed in the study.

Table 5. Mix proportions of the experimental specimens designed in this study.

Sample ID	Fibre vol.% (%)	Water (kg m^{-3})	Cement (kg m^{-3})	Coarse aggregate (kg m^{-3})	Fine aggregate (kg m^{-3})	w/c	Fine aggregate ratio	Superplasticizer[a] (kg m^{-3})	CNT/GNP (kg m^{-3})	Air entrained
Plain	—	238	485	510	951	0.45	0.65	6.1	4.85	0.005
CG-1.0	—	238	485	510	951	0.45	0.65	6.1	4.85	0.005
K-1.0	1	238	485	510	951	0.45	0.65	6.1	4.85	0.005
K-1.5	1.5	238	485	510	951	0.45	0.65	6.1	4.85	0.005
K-2.0	2	238	485	510	951	0.45	0.65	6.1	4.85	0.005
K-2.5	2.5	238	485	510	951	0.45	0.65	6.1	4.85	0.005
PP-1.0	1	238	485	510	951	0.45	0.65	6.1	4.85	0.005
PP-1.5	1.5	238	485	510	951	0.45	0.65	6.1	4.85	0.005
PP-2.0	2	238	485	510	951	0.45	0.65	6.1	4.85	0.005
PP-2.5	2.5	238	485	510	951	0.45	0.65	6.1	4.85	0.005

[a] Polycarboxylate-based superplasticizer.

2.2.4. Compressive test. The measurement of compressive strength was conducted following EN 12504-1, which outlines the testing procedures for evaluating the concrete's compressive strength [48]. In order to meet these requirements, cubic specimens of 150 mm were manufactured after 28 d of the hydration. The average compressive strength was determined by testing at least three specimens. In order to analyse the strain distribution and identify surface discontinuities and potential failures, digital image correlation (DIC) was utilized throughout the loading process. For this specific task, a digital LAVISION M-lite 5 M camera was employed.

2.2.5. Flexural test. Similarly, the average value of three specimens was determined after 28 d. Tests were conducted according to EN 1488 for concrete flexural strength. We, therefore, fabricated specimens with dimensions of 75 mm × 125 mm × 500 mm. A similar method of tying and analysing fibre types was used for the compressive strength tests.

2.2.6. Microstructural assessments. Subsequent to a hydration period of 28 d, the hardened density of the specimens was determined in accordance with the specifications delineated in EN 12390-7. Furthermore, a non-destructive ultrasonic assessment was conducted along the longitudinal axis, employing two probes and adhering to the guidelines outlined in the ASTM C597-16 standard, to examine microstructural properties [1]. Additionally, for the examination of the fracture surfaces of the specimens, scanning electron microscopy (SEM) was employed in the secondary electron mode. Prior to imaging, the specimens were coated with a thin film of Au-Pd (30 nm) through the utilization of a high-resolution sputter coater (Cressington 208 h). Thermal analysis of the specimens was conducted using a thermogravimetric analyzer (TGA, PerkinElmer) under a nitrogen atmosphere (100 Ml min^{-1}), with the maximum temperature reaching up to 1000 °C and a heating rate of 10 °C min^{-1} [43]. To analyze the different cement hydration products and their crystallographic structures, x-ray diffraction analysis (XRD) was employed. XRD analysis is a powerful tool for investigating cement hydration and provides valuable information about phase composition, phase changes, and the progress of hydration. It helps researchers understand the reaction kinetics, identify hydration products, assess the degree of hydration, and evaluate the performance of cement-based materials. For this analysis, the samples were finely ground and sieved to eliminate any sand particles. The x-ray powder diffraction was performed using CuKα ($\lambda = 0.154$ nm) radiation within an angular range spanning from 5 to 80°, with a scanning speed of 3° min^{-1} [33].

2.2.7 Self-sensing assessment. The sensing performance of the composite was evaluated under cyclic compression

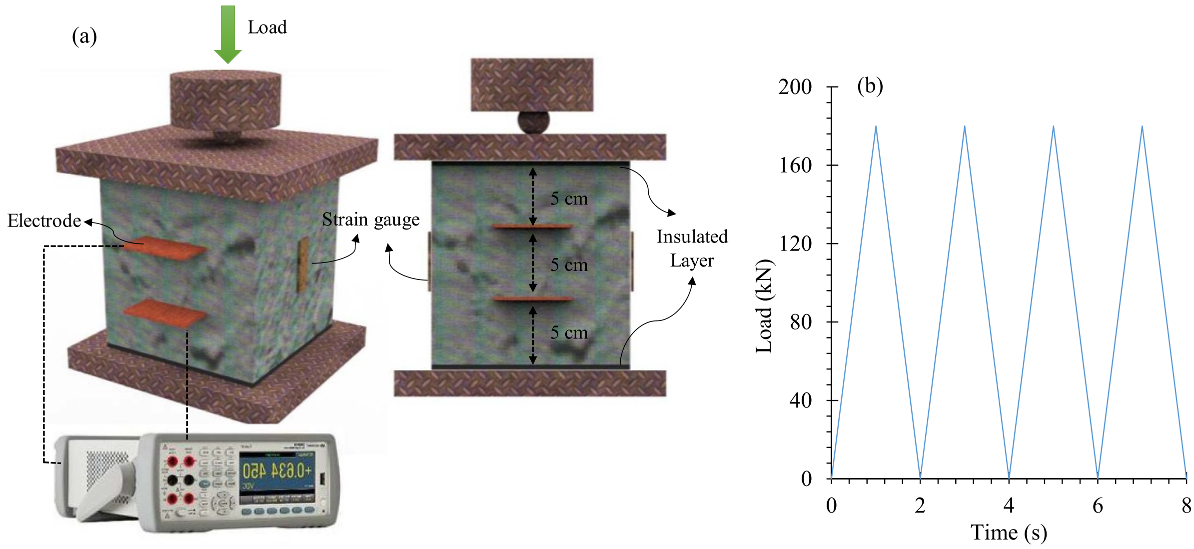

Figure 5. Test setup in piezoresistivity assessment: (a) specimen configuration, (b) cyclic load protocol.

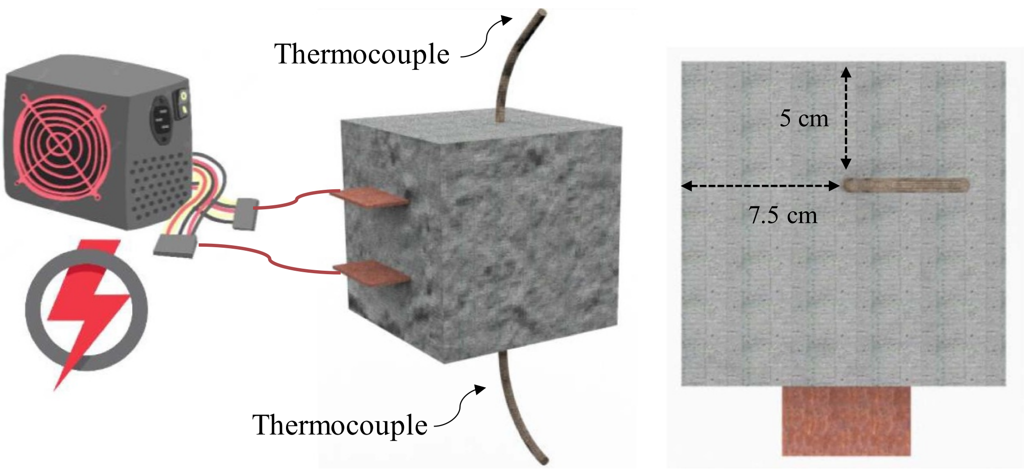

Figure 6. The experimental configuration employed for evaluating self-heating.

loading conditions. In this procedure, illustrated in figure 5(a), cubic specimens of 150 mm containing 2 copper mesh of 50×100 mm (50 mm buried depth), with an Agilent 34 461 A digital multimeter were employed. The loading patterns utilized for this assessment are presented in figure 5(b).

Equations (1)–(3) are employed to obtain fractional changes in electrical resistivity (FCR) and gauge factor (GF).

$$\mathrm{FCR} = \frac{\rho - \rho_0}{\rho_0} \tag{1}$$

$$\rho = R\frac{A}{L} \tag{2}$$

$$\mathrm{GF} = \frac{\mathrm{FCR}}{\varepsilon} \tag{3}$$

where the ρ_0, ρ, A, and L are the initial resistivity, resistivity during the loading, electrodes contact, and distance between electrodes.

2.2.8. Self-heating assessment. The cubic specimens of 150 mm with Power Flex CPX200 D Dual 180 Watt DC supply source were used for the self-heating capabilities assessment as depicted in figure 6. Two holes, each with a length of 50 mm, were drilled into both sides of the specimen, as depicted in figure 6. Thermocouples were then installed into these holes. Subsequently, the holes were resealed with cement paste after the thermocouple installation. A direct current (DC, 25 V) were then applied to the electrodes during the measurement. The thermocouples were placed out of the critical zone of current flow between the two electrodes. This approach aimed to ensure the acquisition of more accurate and realistic temperature increase results.

The average self-heating rate of the composite can be calculated by using equation (4):

$$V_s = \frac{\Delta T_1 - \Delta T_0}{t_s} \tag{4}$$

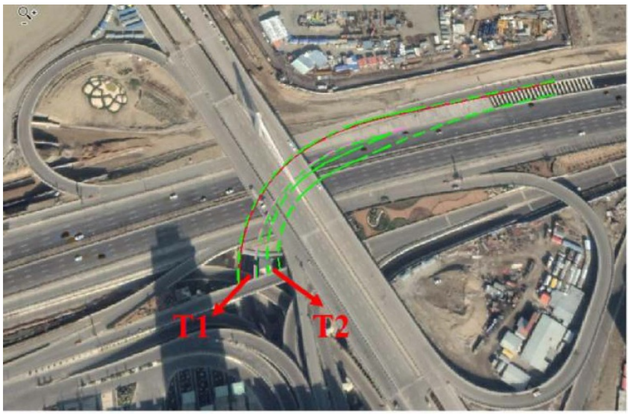

(a)

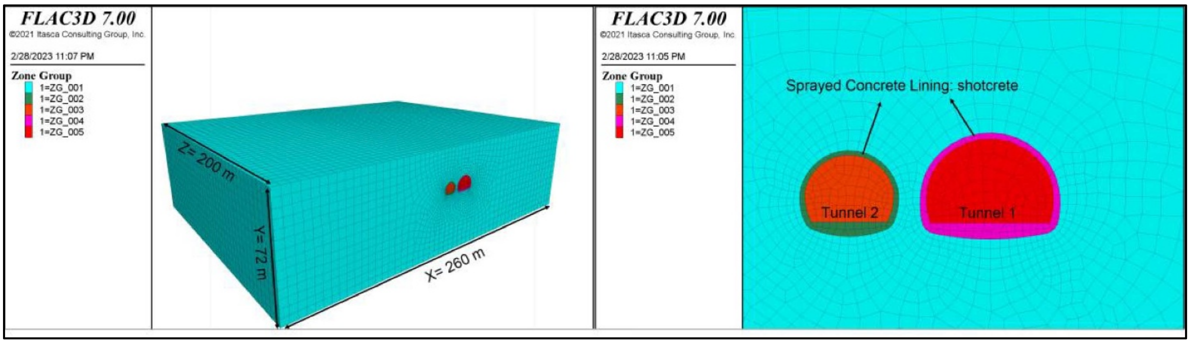

(b)

Figure 7. (a) Route plan for Iran Mall shopping tunnels (b) geometry, dimensions, and meshing of the Iran Mall tunnels numerical model.

where ΔT_1 is the maximum temperature of te slab, ΔT_1 is the initial temperature, and t_s is powering duration.

2.2.9. Numerical analysis with FLAC^{3D} FDM code. FLAC^{3D} is a finite-difference, three-dimensional program intended for the computation of engineering mechanics. Our two-dimensional program, FLAC, provides a well-established numerical formulation for the basis of this program. FLAC^{3D} enhances FLAC's analytical capabilities by extending them into three dimensions, facilitating the simulation of plastic flow occurring within three-dimensional structures constructed from materials such as soil, rock, or other substances when they reach their yield limits. Users have the flexibility to adapt the grid to conform to the shape of the object being modelled by introducing polyhedral elements within it. When subjected to applied forces or boundary constraints, each element follows a predetermined linear or nonlinear stress-strain relationship. The material can undergo yielding and flow, while the grid can deform (in large-strain mode) and move in tandem with the material's behaviour. FLAC^{3D} employs an explicit lagrangian calculation approach and a mixed-discretization zoning method to effectively model plastic deformation and flow. Notably, it accomplishes this without the need for matrices, enabling the execution of large-scale three-dimensional computations without excessive memory consumption. The automatic inertia scaling and automatic damping features address the limitations associated with explicit formulations, such as time-step constraints and damping requirements, all without compromising the capacity to simulate failure modes accurately. Geotechnical engineers can use FLAC^{3D} to solve three-dimensional problems [56].

The efficiency of the optimal proportion of natural fibres in cement shotcrete is assessed through numerical models applied to a twin tunnel within an urban environment. These urban tunnels were constructed to provide parking facilities for visitors of the Iran Mall shopping centre in Tehran, the capital of Iran (see figure 7(a)). Figure 7(b) presents a visual depiction in FLAC^{3D} software illustrating the geometry, dimensions, and meshing of the twin access tunnels (Reference Case). The tunnels possess a length of 200 m, a height of 72 m, and a width of 260 m. Their cross-sectional configuration closely resembles that of a horseshoe, with the tunnels positioned in close proximity to one another. To ensure heightened precision, additional and denser meshes are employed around the tunnels. The larger tunnel is designated as 'number 1', while the smaller tunnel is denoted as 'number 2'. In the context of numerical modelling for the tunneling process and the accurate prediction of lining loads, selecting an appropriate constitutive model for the soil mass assumes paramount significance. It should be noted that employing a constant stiffness approach would be unsuitable for approximating surface settlements across all levels of shear strain [57, 58]. The plastic hardening constitutive model employed in this study is typified

Table 6. Plastic hardening model and physical properties of the soil mass.

Parameters	Symbol	Unit	Value
Density	ρ	kg m^{-3}	2000
Cohesion	C	kPa	20
Internal friction angle	φ	Degree	35
Angle dilation	ψ	Degree	5
The Young's modulus of triaxial loading secant	E_{50}^{ref}	Mpa	120
Reloading and unloading Young's modulus	E_{ur}^{ref}	Mpa	240
Young's modulus of Oedometric loading	$E_{\mathrm{oed}}^{\mathrm{ref}}$	MPa	96
Coefficient of earth lateral pressure	K_0	—	0.42
Poisson's ratio	ν	—	0.27
Failure ratio	R_f	—	0.9
Janbu-type parameter	m	—	0.5
Reference mean pressure	P_{ref}	kPa	100

Table 7. Mechanical and physical properties of the shotcrete tunnel lining.

Shotcrete	Poisson's ratio	Young's modulus (GPa)	Tensile strength[a] (MPa)	Compressive strength (MPa)	Density (kg m^{-3})	Flexural strength (MPa)
Without fibres	0.2	30.7	3.3	49.5	2408	4.15
With Kenaf (1.5%)	0.22	31.4	4.8	44.7	2382	7.6
With PP (2%)	0.2	30.1	4.1	41.6	2260	5.3

[a] Splitting tensile strength (STS) Based on ASTM C496/C496M.

by a hyperbolic stress-strain relationship during drained axial compression, with elasticity governing unloading/reloading, and stress-dependent behaviour governed by a power law. This model also encompasses shear and volumetric hardening, along with the utilization of the Mohr-Coulomb (MC) failure criteria. The soil compressibility is explained by three nonlinear rigidities contingent on the stress level ($E_{50}^{\mathrm{ref}} - E_{\mathrm{oed}}^{\mathrm{ref}} - E_{ur}^{\mathrm{ref}}$) [59].

Tables 6 and 7 present the mechanical and physical properties of the soil surrounding the tunnel and its shotcrete lining. As mentioned, the soil mass and shotcrete lining were modelled using the Plastic Hardening constitutive model and MC failure criteria, respectively. In the simulation of shotcrete with fibres, the MC constitutive model was employed to account for the requisite strength parameters. Thus, we have considered the influence of fibres within the tunnel lining using an indirect method in FLAC3D. Indeed, the modelling was conducted considering the impact of fibres on the physical and mechanical properties of concrete, rather than modelling the individual behaviour of the fibre within the cementitious matrix [60]. By applying the MC constitutive model to the mesh elements (solid elements) of the tunnel lining, we can define elastic and strength parameters for shotcrete without fibres and shotcrete with fibres. Table 7 shows the strength and physical characteristics of shotcrete without fibres and with the optimum percentage of the fibres made of Kenaf and PP, obtained from the lab tests (section 3.1).

To conduct the numerical analysis, the initial equilibrium of the numerical model must be achieved, enabling the calculation of the desired stress ratio. Following that, the tunnel section is excavated sequentially using the Austrian method, with each stage involving a one-meter excavation step. Immediately following excavation, shotcrete (sprayed concrete lining) is applied. As part of the modelling process, the twin tunnels are simultaneously excavated under critical conditions with an applied normal load equivalent to the building's surface load (80 kPa). In this manner, the excavation process is repeated until a total excavation length of 200 m is reached. The results of the numerical analysis will be presented in the following sections.

Furthermore, in this study, we utilized harmonic seismic loading characterized by a maximum acceleration of 0.02 g (PGA = 0.02 g) and lasting for a duration of 15 s. This approach was adopted to assess the impact of fibre-reinforced concrete shotcrete on the displacement and dynamics of shotcrete tunnels. It is important to note that the assumed harmonic load frequency in this investigation was 0.75 Hz. As illustrated in figure 8, the lateral boundaries of the dynamic numerical model were treated as free-field boundaries to account for both absorbing and infinite boundary conditions [56, 58]. Additionally, in order to incorporate the influence of the bedrock on the lower boundary of the numerical model, the lower boundary was regarded as fixed and rigid [61]. A fish FLAC^{3D} language was used for entering the seismic load in the form of harmonic acceleration history into the lower boundary of the tunnel model in order to calculate the dynamic load. To dissipate the earthquake, wave propagation, hysteresis damping was applied to the soil surrounding the tunnel. Rayleigh damping was also used in the shotcrete of the tunnel as a form of damping.

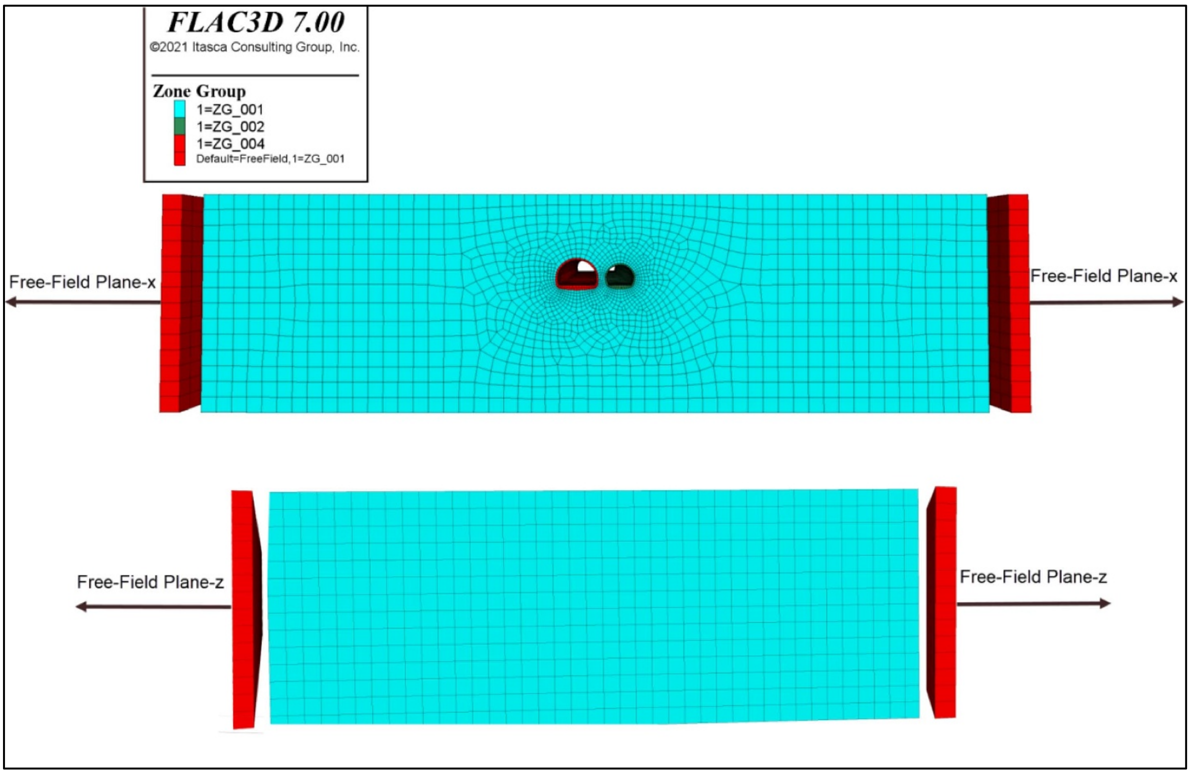

Figure 8. Dynamic boundary conditions in the lateral boundaries of the 3D model.

3. Results and discussion

3.1. Self-sensing assessment

The variation of DC resistivity for the concrete composites reinforced with Kenaf and PP fibres is shown in figure 9. The electrical resistance of the sample lacking CNT/GNP exceeded the measurable range of our equipment. In both reinforcement scenarios involving Kenaf and PP fibres, elevating the fibre concentration results in a corresponding rise in the electrical resistance of the composites. The findings revealed a progressive increase of approximately 10%, 63%, 113%, and 196% in the DC resistivity of the composite with the incorporation and augmentation of Kenaf fibre concentration from 1.0% to 1.5%, 2.0%, and 2.5%, respectively. Similarly, elevating the PP fibre concentration from 1.0% to 1.5%, 2.0%, and 2.5% resulted in an approximate rise of 42%, 103%, 186% and 268% in the DC resistivity of the composite. Conductive pathways in hybrid CNT/GNP-reinforced cementitious composites are formed through the synergistic integration of these nanomaterials. Graphene nanoplatelets create overlapping layers, and carbon nanotubes align within the matrix, forming a cooperative network that facilitates electron movement. Simultaneously, percolation and electron tunneling effects play fundamental roles, marking the transition to electrical conductivity and enhancing overall electron transport. The synergy of these effects defines the electrical behaviour of the composite material. Kenaf and PP fibres, known for their insulating properties, introduce a higher volume fraction of non-conductive elements into the composite, hindering the flow of electrical charge. This increased content of insulating fibres can disrupt the continuous conductive network formed by CNTs and GNPs, leading to less efficient electron pathways and a subsequent rise in electrical resistivity. Interactions at the interfaces between fibres and conductive nanomaterials, along with the cumulative effects of volume fraction adjustments, contribute to the overall increase in electrical DC resistivity in the composite. Achieving a balance between conductive and insulating components is crucial for tailoring the electrical properties of the composite to meet specific application requirements.

Figure 10 shows strain and FCR versus time plots for the composites reinforced with Kenaf an PP fibres. Under cyclic compressive loading, the observed negative values of the FCR suggest a reduction in the material's electrical resistivity during compression cycles. This phenomenon can be attributed to the compression-induced alignment or reorientation of conductive elements within the material. As the material undergoes compression, the conductive pathways likely become more organized, leading to increased electrical conductivity and, consequently, a decrease in resistivity. The increase in the absolute value of FCR at the peak of loading indicates a heightened sensitivity of the material to mechanical forces during compression peaks, inducing more pronounced changes in the arrangement of conductive elements. This results in a substantial fractional change in resistivity. On the contrary, the reduction in the absolute value of FCR at the end of cyclic loading suggests a partial recovery of the material's initial electrical resistivity during the relaxation phase, as the conductive elements may relax or reorient. These dynamic

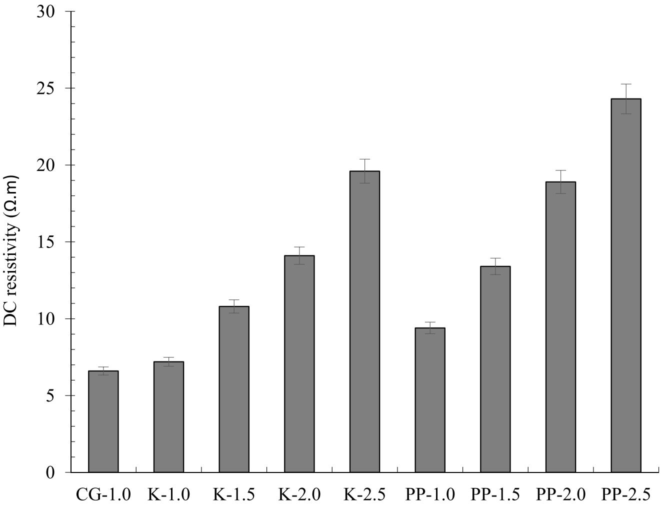

Figure 9. DC resistance of the composite reinforced with kenaf and PP fibres.

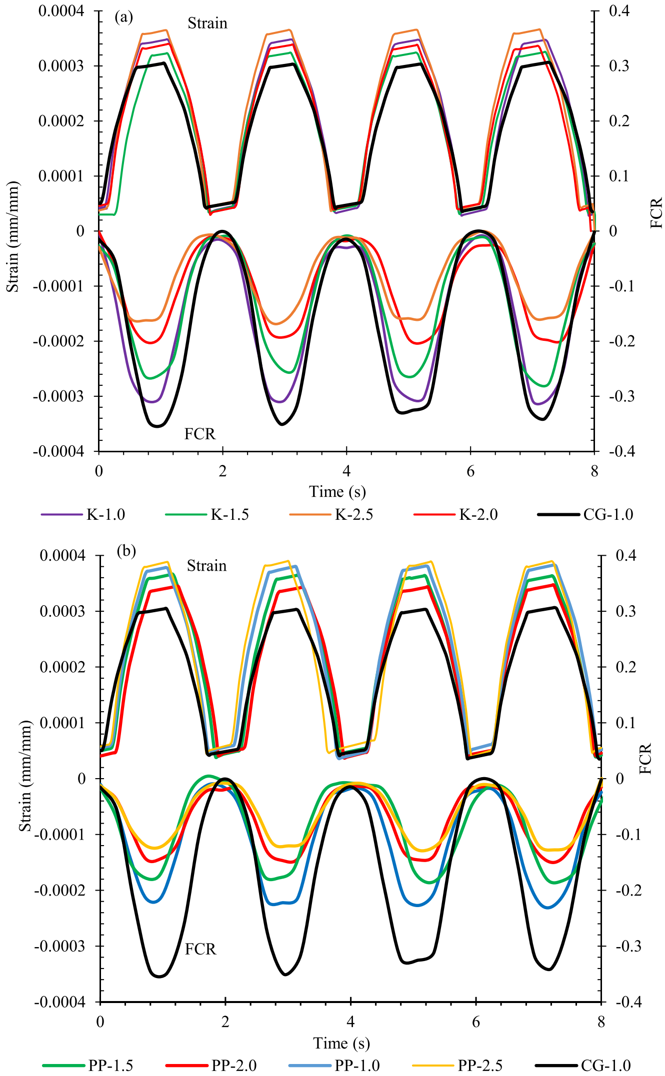

Figure 10. Strain–time–FCR curves under compression cyclic loading: (a) reinforced with Kenaf fibre, (b) reinforced with PP fibre.

variations underscore the material's adaptability and reversible changes in electrical properties in response to varying mechanical loading conditions. The findings indicated that the composite reinforced with PP fibres exhibited lower absolute values of the FCR in comparison to the composite reinforced with Kenaf fibres. Incorporation and elevating the Kenaf fibre concentration from 1.0% to 1.5%, 2.0%, and 2.5% resulted in a decline in the absolute values of the FCR at the peak of loading cycles by approximately 12%, 26%, 45%, and 56% respectively. Meanwhile, augmenting the PP fibre concentration from 1.0% to 1.5%, 2.0%, and 2.5% induced a comparatively greater reduction in the absolute FCR values, yielding decreases of around 36%, 48%, 57%, and 64% respectively.

The incorporation and heightened concentration of Kenaf and PP fibres within a conductive cement-based composite, act as influential factors in reducing the absolute value of maximum FCR observed at the peak of cyclic compression loading. The fibres influence contact resistance between conductive elements, introducing resistance and diminishing overall conductivity. As a result, the effects of increased fibre concentration alter the balance between conductive and insulating components, leading to a reduction in the absolute value of maximum FCR. This complex interplay highlights the intricate relationship between material composition and electrical behaviour during cyclic compression loading, emphasizing the insulating influence of fibres in the composite. However, PP fibres tend to increase the DC resistivity more than Kenaf fibres in a composite containing hybrid CNT/GNP due to inherent differences in the electrical properties of these fibres. PP fibres, being synthetic, typically possess higher electrical resistivity compared to natural fibres like Kenaf. The molecular structure of PP and its insulating nature contribute to impeding the flow of electrical charge more significantly than Kenaf fibres. Additionally, the synthetic origin of PP fibres may introduce fewer conductive pathways, causing a more pronounced disruption in the overall conductive network formed by CNTs and GNPs in the composite. In contrast, Kenaf fibres, being of natural origin, may exhibit relatively lower resistivity and could contribute fewer impediments to the conductive network, resulting in a comparatively lesser increase in DC resistivity when incorporated into the composite.

Figure 11 illustrates the strain GFs for the composite reinforced with both Kenaf and PP fibres. The outcomes indicated a consistent decrease in strain GFs with the incorporation and progressive increase in both Kenaf and PP fibre concentrations. Notably, the reduction in strain GFs was more pronounced when reinforcing with PP fibres.

3.2. *Self-heating assessments*

Temperature time histories of the composites reinforced with Kenaf and PP fibres are depicted in figure 12. As results showed, initially, when the voltage was applied, the temperature rose steadily due to the joule heating effect, where electrical energy is converted into heat within the composite. This phase reflects an increasing temperature gradient until thermal equilibrium is reached. Once thermal equilibrium was

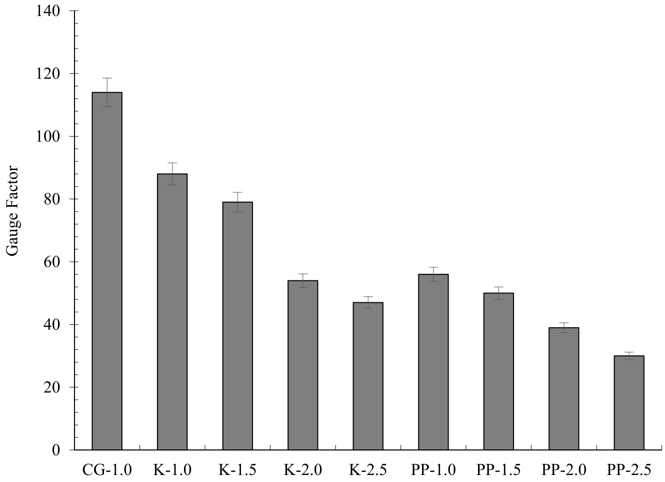

Figure 11. Gauge factors under compression cyclic loading for composites reinforced with Kenaf and PP fibres.

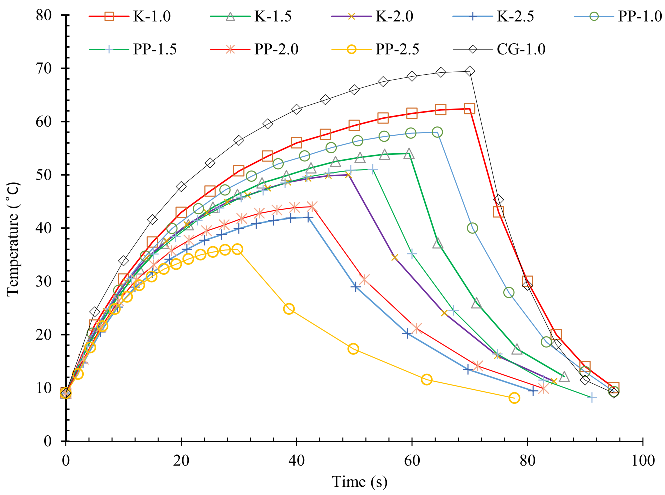

Figure 12. Temperature time histories of the composites reinforced with Kenaf and PP fibres.

attained, the temperature stabilized, forming a plateau as the heat generated by joule heating is balanced by heat dissipation and other thermal processes within the material. At this stage, disconnecting the voltage would lead to a cessation of the joule heating effect. Subsequently, after disconnecting the voltage, the temperature-time history demonstrated a gradual decrease as the system undergoes cooling. The rate of cooling depends on the thermal properties of the composite and its surroundings. The trend might exhibit an exponential decay as the material returns to ambient temperature. The incorporation and elevation of Kenaf fibre concentration from 1.0% to 1.5%, 2.0%, and 2.5% resulted in a decrease in heating rate by approximately 12%, 21%, 25%, and 36%, respectively. Conversely, for PP fibre, the corresponding reductions were approximately 18%, 23%, 31%, and 34% with the incorporation and increase in concentration from 1.0% to 1.5%, 2.0%, and 2.5%, respectively.

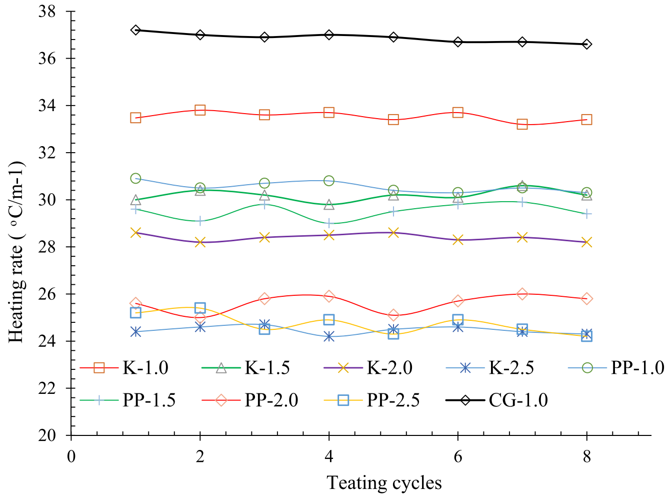

Figure 13. Average self-heating rate after 8 joule heating cycles.

As results showed, the progressive increase in Kenaf and PP fibre concentration within the conductive cement composite contributed to a reduction in the peak temperature and heating rate during joule heating. This phenomenon stems from the insulating properties of Kenaf and PP fibres, which impede the efficient flow of electrical current and subsequently decrease the rate at which electrical energy is converted into heat. As the fibre concentration rises, the conductive network formed by CNTs and GNPs is disrupted, leading to increased electrical resistance and diminished joule heating efficiency. This disruption not only results in a slower heating rate but also influences the maximum temperature attained under the same voltage. The insulating nature of Kenaf and PP fibres restricts the extent of temperature elevation, as a higher fibre concentration introduces more non-conductive elements, hindering the propagation of heat. Moreover, the cooling rate after disconnecting the voltage is also reduced, reflecting the altered thermal dynamics within the composite. These combined effects underscore the intricate interplay between fibre concentration and the electrical and thermal behaviour of the CNT/GNP cement composite, emphasizing the crucial role of fibre content in modulating joule heating characteristics.

Figure 13 illustrates the average self-heating rate observed in both Kenaf and PP fibre-reinforced composites throughout 8 cyclic joule heating.

As can be observed the incorporation and progressive increase in Kenaf and PP fibre concentration introduced a slight reduction in the stability of the heating rate during joule heating, particularly evident after eight cyclic heating events. This reduction in stability can be attributed to changes in the physical properties of the composite. As fibre concentration increases, alterations occur in the structural integrity, thermal conductivity, and electrical resistivity of the composite material. The introduction of non-conductive fibres disrupts the uniformity of the conductive network formed by CNTs and GNPs, leading to variations in electrical and thermal pathways. These changes in physical properties result in non-uniform heating and altered heat dissipation characteristics during successive joule heating cycles. The uneven distribution and orientation

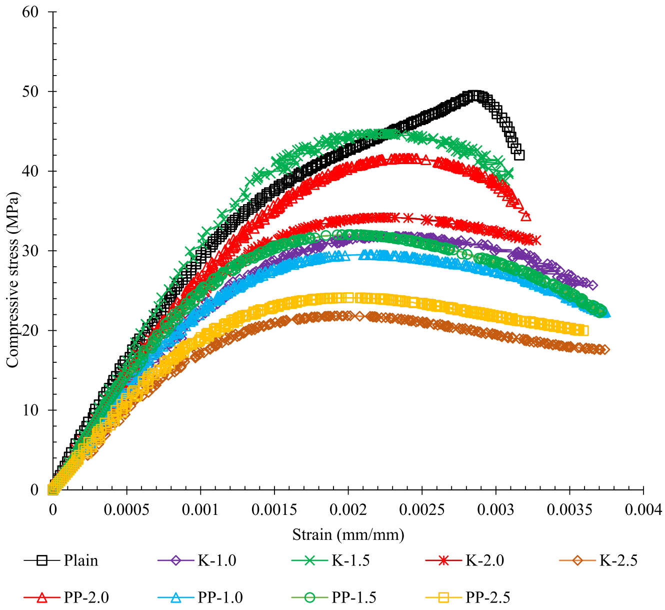

Figure 14. The stress-strain curves of the shotcrete reinforced with fibres.

of fibres introduce spatial heterogeneities, contributing to fluctuations in the heating rate and, consequently, reducing the stability of the heating process. Therefore, the observed instability can be attributed to the complex interplay of physical property changes induced by the incorporation and increasing concentration of fibres in the CNT/GNP cement composite.

3.3. Mechanical assessment

Figure 14 presents the stress-strain curves for concrete reinforced with Kenaf and PP fibres at various concentrations. The outcomes reveal an enhancement in the ductility characteristics of the composite influenced by the addition of fibres. The results showed an improvement in the ductility behaviour of the composite affected by fibre reinforcement. Particularly, the incorporation of the fibres into the concrete significantly enhanced the post-crack region of the composite due to the higher dissipated energy caused by the crack bridging and divination mechanism of the fibres.

The enhancement of ductility in cementitious composites following the incorporation of fibres, stems from the reinforcing mechanisms imparted by these fibres. Acting as bridges across cracks, the fibres redistribute stress and strain, impeding crack propagation and facilitating greater deformation before failure [36, 40]. The post-crack load transfer capability of the composite is improved as fibres continue to support the material even after cracks have formed, and their length and orientation contribute to more effective stress resistance. Additionally, fibres introduce energy dissipation mechanisms, such as pull-out and debonding, mitigating the severity of crack propagation and augmenting the material's overall ductility [43]. The nature of the fibre-matrix interaction, including proper bonding, further ensures that the fibres positively influence the composite's mechanical behaviour [62]. Careful consideration of fibre type and aspect ratio is essential to optimize ductility without compromising other material properties. Concisely, the improved ductility of fibre-reinforced cementitious composites arises from a synergistic interplay of various mechanical mechanisms that enhance the material's ability to deform before ultimate failure.

Figure 15 depicts the compressive stress values for shotcrete reinforced with varying concentrations of Kenaf and PP fibres. A general reduction in compression strength was observed in the composites when Kenaf and PP fibres were incorporated. Similar trends were reported in the literature [63]. The addition of fibres, can disrupt the homogeneity of the cementitious matrix. This disruption leads to the formation of pores during the mixing and curing processes. Pore formation is often a consequence of inadequate compaction and an uneven distribution of fibres within the matrix. The presence of pores acts as stress concentration points, weakening the composite and diminishing its compressive strength [36, 40]. The physical performance of cementitious composites is closely tied to their structural integrity and density. The incorporation of low-density fibres may compromise the matrix's ability to form a tightly packed structure [43]. This phenomenon occurs due to the relatively lower density of the fibres compared to the surrounding matrix. The presence of voids and pores within the composite structure adversely affects its overall density and hinders the efficient transfer of compressive forces. As a result, the compressive strength can be adversely affected [64]. This impact on physical performance is exacerbated when the fibre concentration is high, leading to a more pronounced reduction in compression strength. At higher fibre concentrations, the structural arrangement within the composite undergoes significant changes. The irregular distribution of fibres may lead to clustering or agglomeration, further exacerbating the formation of voids. These structural irregularities negatively impact the composite's ability to withstand compressive loads [1].

As shown in figure 15, the incorporation of 1.0%, 1.5%, 2.0%, and 2.5% of the Kenaf fibres into the concrete, reduced the compressive strength by around 36%, 9.0%, 31%, and 56% respectively. This trend indicates the maximum compressive strength for specimen K-1.5 which contained 1.5% of the Kenaf fibres. Meanwhile, the addition of the PP fibres into the composite with equal percentages reduced the compressive strength by around 40%, 35%, 16%, and 51% respectively. In the case of PP fibres, the maximum compressive strength was obtained for the specimen PP-2 which was composed of 2% PP fibres. Indeed, the optimum percentages of the PP fibres were more than Kenaf, which might be related to the diameters (aspect ratio) of the fibres. However, it is noteworthy that the composite containing the optimal concentration of Kenaf fibre exhibited a higher maximum compressive strength compared to that of PP.

Figure 16 shows the compression elastic modulus of the concrete composed of different Kenaf and PP percentages. The results showed the maximum elastic module for the specimens K-1.5 and PP-2 which were relatively equal to the plain sample. Indeed, incorporation of the 1.0%, 1.5%, 2.0%, and 2.5% of the Kenaf fibres into the concrete reduced the elastic

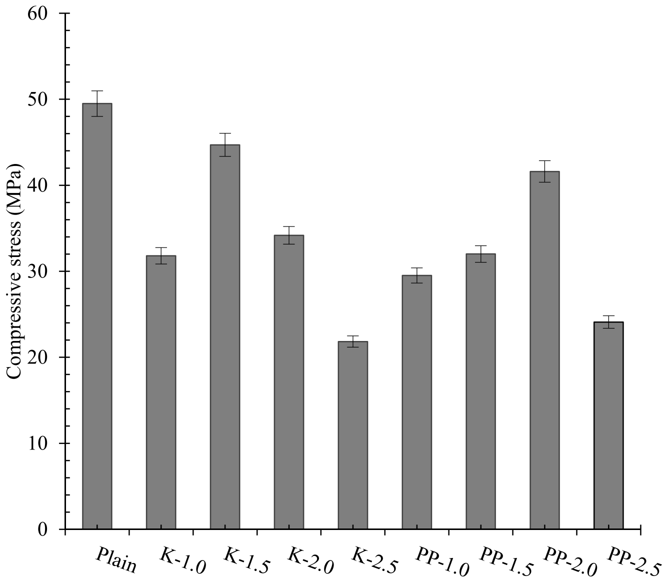

Figure 15. The compressive stress of the shotcrete reinforced with fibres.

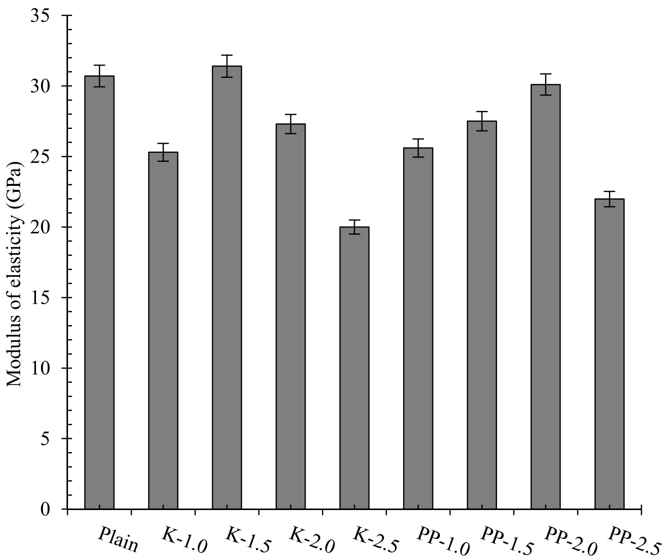

Figure 16. Elastic modulus of the shotcrete reinforced with fibres.

module by around 17.0%, 1.0%, 11%, and 35% respectively compared to the plain specimen. In the case of PP, the elastic module was reduced by around 16%, 10%, 2.0%, and 28% respectively.

The rapture modulus of shotcrete reinforced with different concentrations of Kenaf and PP fibres in compressive conditions is presented in figure 17. Generally introducing the fibres into the concrete caused an improvement in ductile behaviour and consequently the rapture modulus of the composite. This might enhance the mechanical performance of the composite in the post-crack region [36, 40]. As can be observed, the incorporation of the 1.0%, 1.5%, 2.0%, and 2.5% of the Kenaf fibres into the concrete improved the rapture modulus of the composite by approximately 20%, 45%, 36%, and 21%, approximately compared to the plain specimen. In the case of

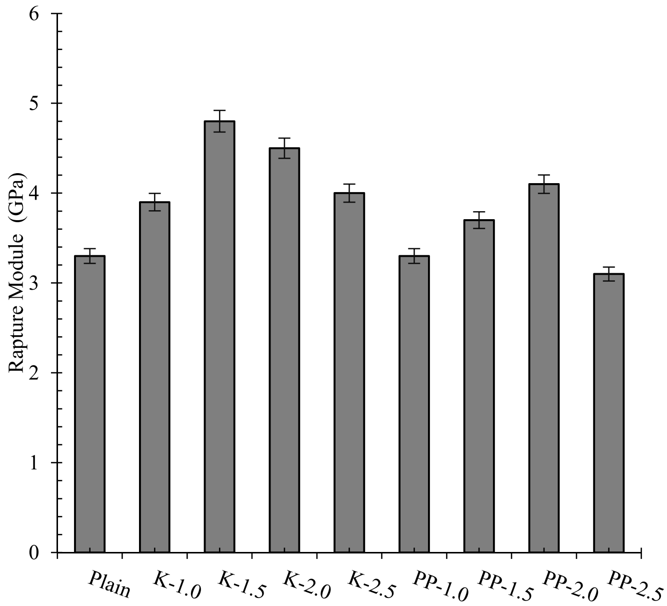

Figure 17. Rapture modulus of the shotcrete reinforced with fibres.

PP fibre, the rapture modulus of the composite showed no significant changes. Just in specimens PP-1.5 and PP-2, we can see a 12% and 25% of improvement.

The analysis of the captured digital images for specimens K-1.5 and PP-2.0, corresponding to the first crack and failure steps are also illustrated in figure 18.

As can be observed both PP-reinforced concrete and Kenaf-reinforced concrete could improve crack control. The fibres in both cases help distribute stress and limit crack propagation. PP fibres are synthetic fibres known for their high tensile strength, impact resistance, and durability. On the other hand, Kenaf fibres are natural fibres with lower tensile strength and stiffness compared to synthetic fibres. However, DIC results for Kenaf-reinforced concrete demonstrated better crack control and strain localization due to the proper interaction of the Kenaf fibres and cement-based matrix.

Figure 19 illustrates the flexural strength of concrete reinforced with varying concentrations of Kenaf and PP fibres under compressive conditions. In comparison with plain concrete, the composites reinforced with 1.0%, 1.5%, 2.0%, and 2.5% of Kenaf fibres, showed an improvement in flexural strength by approximately 56%, 83%, 30%, and 10% respectively.

It is evident from the data that the introduction of PP fibres into the composite led to a substantial enhancement in flexural strength, particularly in specimens PP-1.5 and PP-2, where the increase was approximately 20% and 28%, respectively. Generally reinforcing the cement-based composites with a certain amount of the fibres can increase the flexural strength through the crack bridging and/or deviation. However, an excessive increase in the fibre concentrations increases the porosity of the composite due to the agglomeration formation and reduces the flexural strength [41, 49, 65]. The augmentation of flexural strength in cement-based composites through fibre reinforcement can be rooted in several

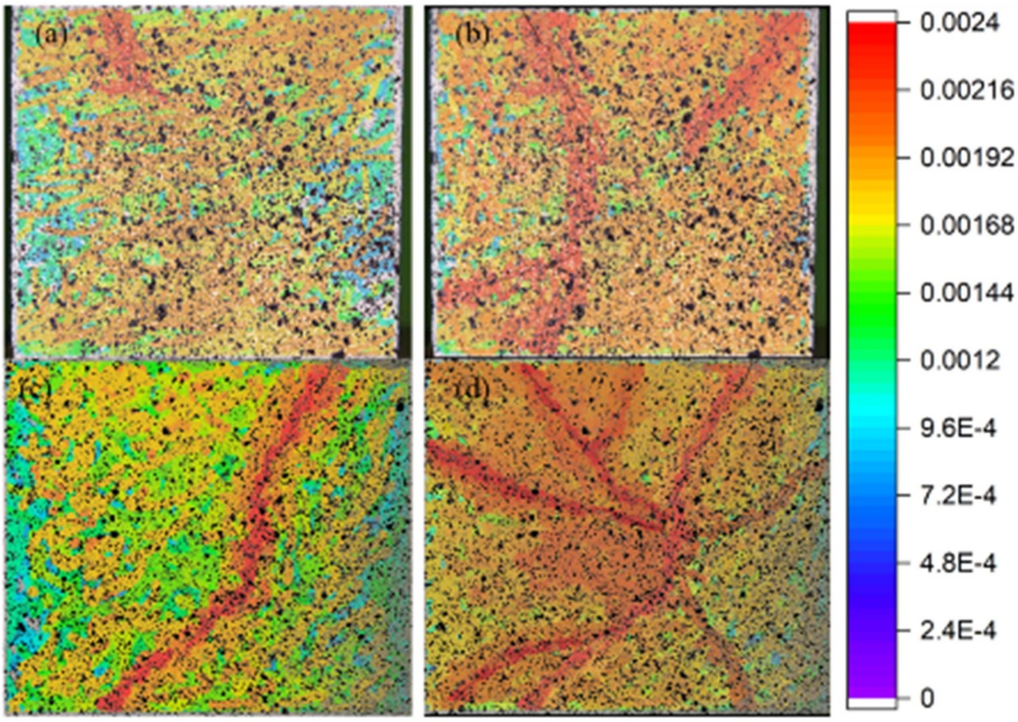

Figure 18. DIC analysis of the typical strain distribution at different stages of compression: (a) specimen K-1.5 (first crack), (b) specimen K-1.5 (a moment before the failure), (c) specimen PP-2.0 (first crack), (d) specimen PP-2.0 (a moment before the failure).

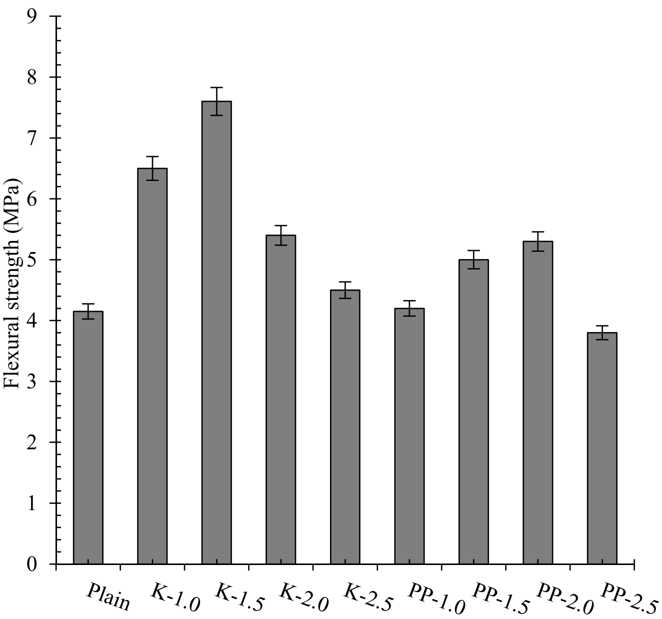

Figure 19. Flexural strength of the shotcrete reinforced with fibres.

fundamental mechanisms. As discussed, fibres, whether synthetic or natural, act as effective crack arrestors, redistributing stress and preventing crack propagation during flexural loading. This crack-bridging capability, combined with the increased toughness and energy absorption provided by fibres, enhances the material's ability to withstand bending stresses, leading to improved flexural strength. The inherent ductility and enhanced strain capacity afforded by fibre reinforcement play a pivotal role in allowing the composite to undergo greater deformation before failure, contributing further to elevated flexural strength. Factors such as fibre length and orientation, matrix-fibre interface bonding, and the post-crack load transfer mechanism further optimize the composite's response to flexural loads, collectively resulting in the observed increase in flexural strength.

The proper interaction of the cement-based matrix with the natural fibres interface due to surface texture and proper chemical bonding of the cement hydration products with natural fibres, increase their performances in crack propagation prevention and consequently increase the flexural strength [1, 42].

3.4. Microstructural analysis

3.4.1. Hardened density. Figure 20 displays the hardened density of the concrete reinforced with varying concentrations of Kenaf and PP fibres. Introducing 1.0%, 1.5%, 2.0%, and 2.5% of the Kenaf fibres into the concrete, reduced the hardened density of the composite by approximately 21%, 3%, 13%, and 27%. As shown in figure 20, the incorporation of the PP percentages with equal percentages, reduced the hardened density of the specimens by around 21%, 12%, 6.0%, and 25% respectively. These results are consistent with the mechanical assessment. As previously discussed in section 3.1, the incorporation of low-density fibres into the composite typically results in a reduction in overall density. The excessive increases in fibre percentages also increase the porosities by increasing the gaps and distances between the aggregates.

In general, adding fibres to cement-based composites tend to slightly increase their density. The fibres are typically mixed

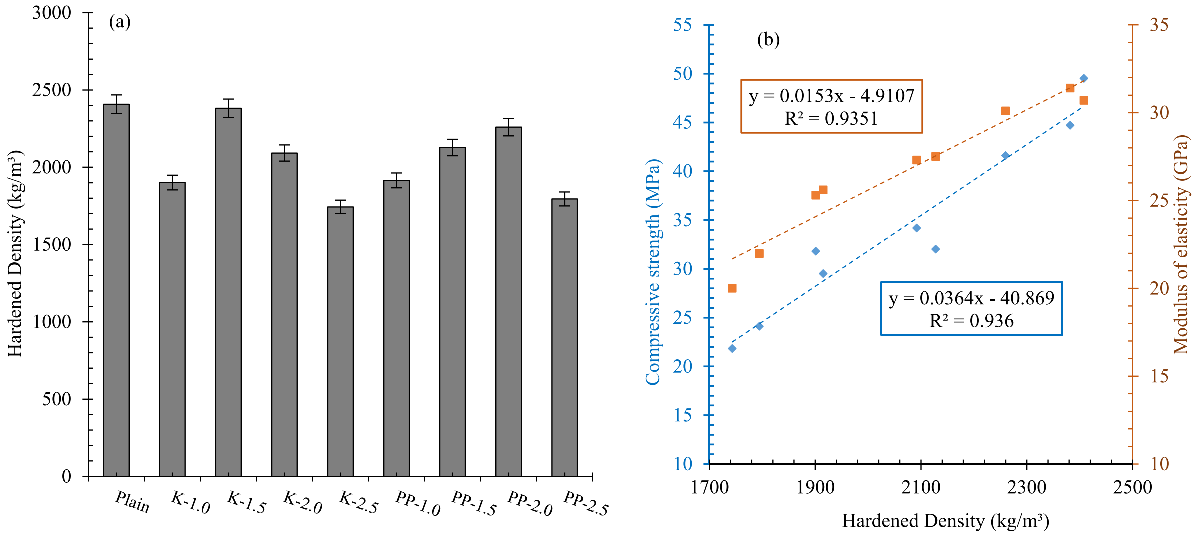

Figure 20. (a) The hardened density of the shotcrete reinforced with fibres, (b) correlation between hardened density, compressive strength, and modulus of elasticity.

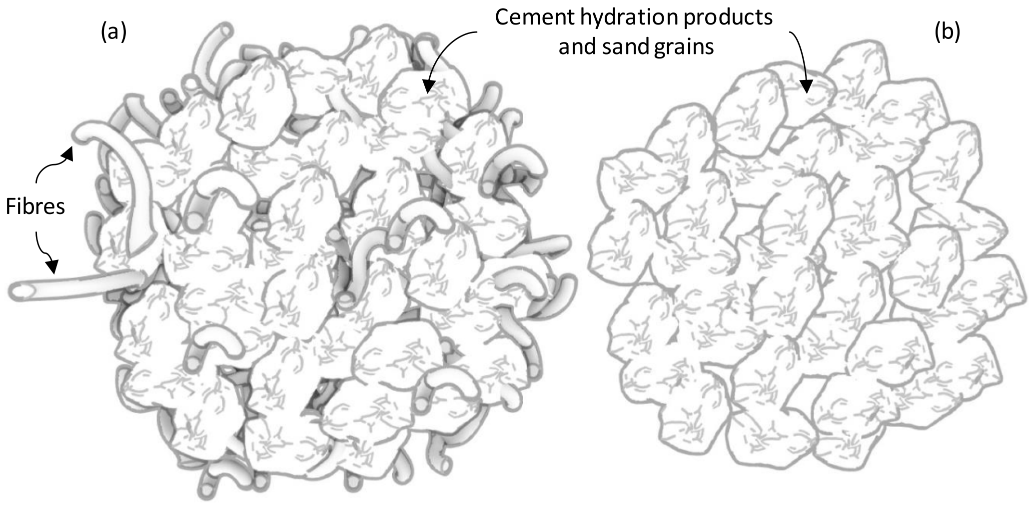

Figure 21. A schema of fibres filler mechanism in cement-based composites: (a) reinforced with fibres, (b) without fibres.

into the cement-based mixture, which can displace some of the air voids and reduce the overall porosity (figure 21). As a result, the composite becomes more compact, leading to a higher density. However, it is pertinent to acknowledge that the increment in density resulting from the inclusion of fibres is generally marginal, often insufficient to exert a significant influence on the overall properties of the concrete.

3.4.2. Ultrasonic wave time passing. Figure 22 presents the results of ultrasonic wave transit times for fibre-reinforced composites featuring various fibre types and concentrations. A cement-based composite's physical properties can be assessed indirectly by ultrasonic pulse velocity testing [47]. In this test, an ultrasonic pulse is employed to assess the strength and density of cement-based composites by measuring the time it takes for the pulse to traverse the matrix structure [36, 49]. The outcomes for both types of fibre-reinforced composites revealed an increase in wave transit time, especially with rising fibre concentrations. This phenomenon can be attributed to the diminishing density of the composites. As fibre concentration increases, the composite's density decreases, thereby extending the time taken for the ultrasonic wave to pass through. Notably, these findings align with the observations made in the preceding section, which discussed hardened densities and mechanical properties.

3.4.3. Fibres impact on formation rate of cement hydration products. The results of the XRD analysis for the samples containing 1.5% Kenaf (K-1.5) and 2.0% PP (P-2.0) are shown in figure 23. These two compositions were the optimum composition based on the physical, mechanical, self-sensing, and self-heating assessment discussed in previous sections.

The results demonstrate a general increase in hydration products following the inclusion of CNT/GNP. Indeed, CNT and GNP act as nucleation sites for the formation of hydration products. Their high surface area provides ample sites for

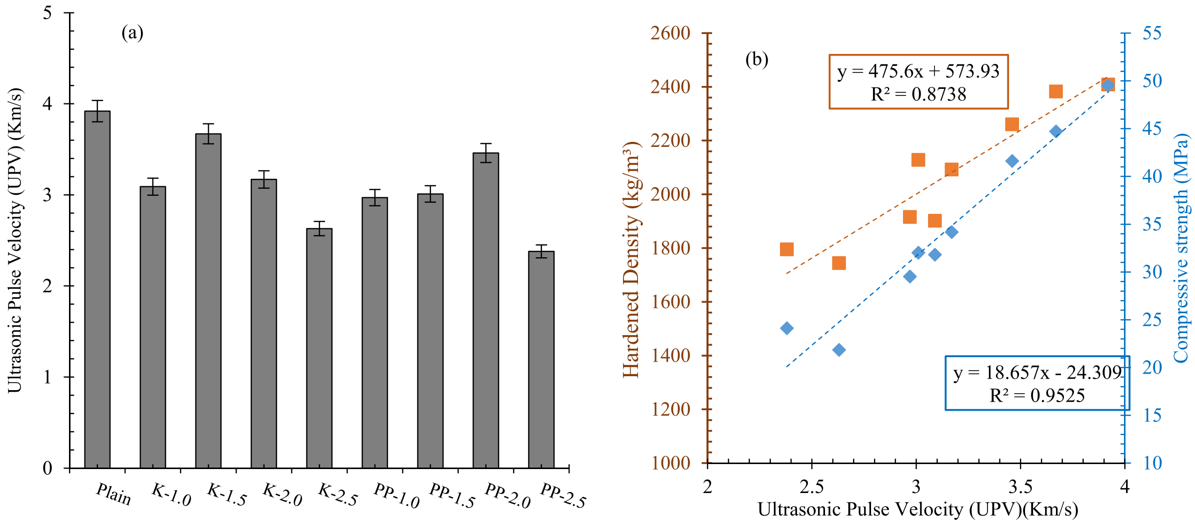

Figure 22. (a) Ultrasonic pulse velocity (UPV) of the shotcrete reinforced with fibres, (b) correlation between UPV, hardened density, and compressive strength.

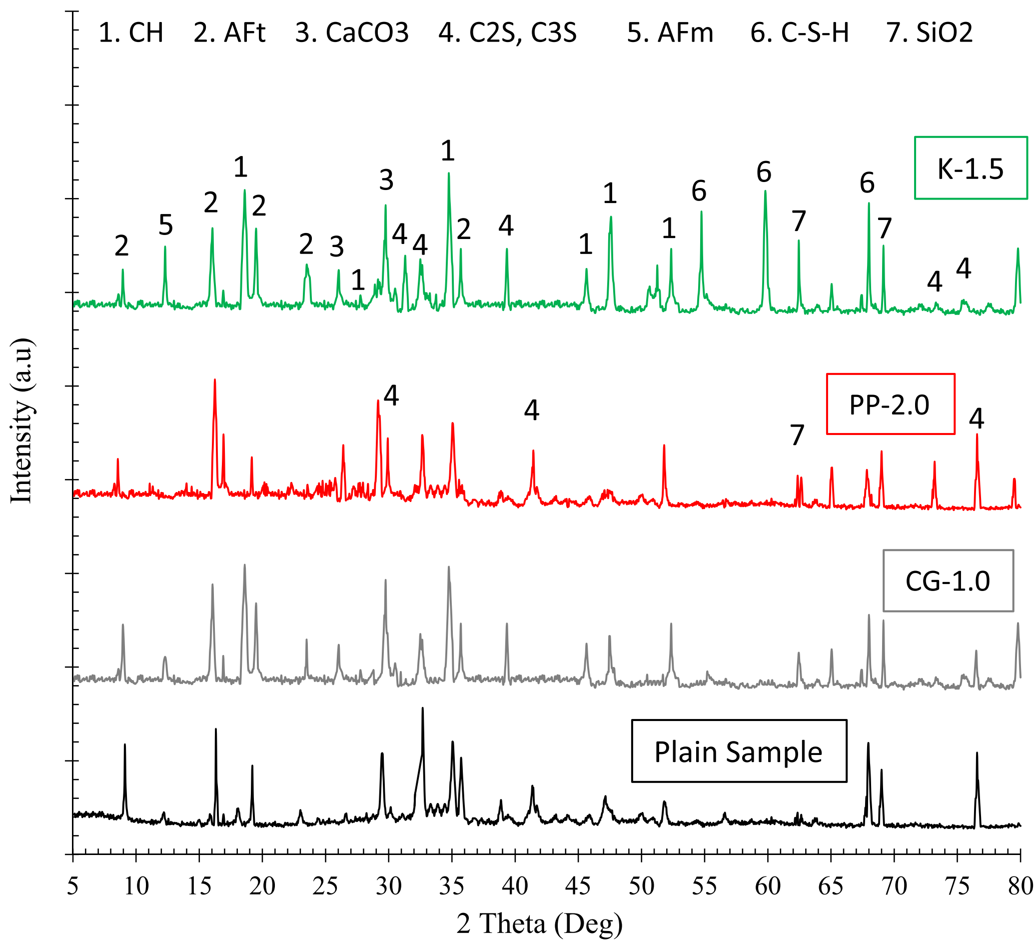

Figure 23. XRD spectra for the specimen reinforced with 1.5% Kenaf (K-1.5) and 2.0% PP (P-2.0).

the deposition and growth of hydration products, accelerating the nucleation process and promoting denser cementitious microstructures [47, 66].

It is evident that the introduction of Kenaf fibres into the cement-based composite resulted in a slight increase in the formation of hydration products, including AFm, AFt, CH, and C-S-H. However, the inclusion of PP fibres did not exhibit a significant impact on the rate of cement hydration. Based on the literature, the non-treated natural fibre can delay the hydration process due to the presence of lignin in cement composites

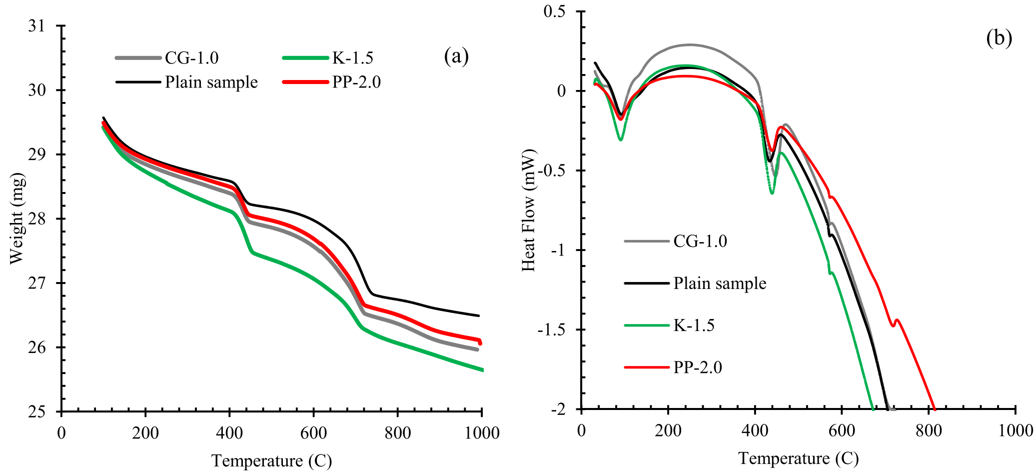

Figure 24. Thermal analysis of the specimen containing 1.5% Kenaf (K-1.5) and 2.0% PP (P-2.0): (a) TGA graphs, (b) DSC graphs.

[52]. However, the chemical treatment involves modifying the fibre's hydroxyl groups and introducing other interacting groups such as oxygen functional groups that effectively bond with the cement hydration products at the interface. Meanwhile, the absorbed water at the surface of the fibres also provides a suitable platform for the formation and growth of hydration products [43, 47]. Indeed the Kenaf fibres also likely act as nucleation sites for the precipitation of hydration products during the early stages of cement hydration [43]. The fibres may provide surfaces that encourage the adsorption and growth of hydrates, such as AFt and AFm phases, leading to a more pronounced development of these cementitious phases. Additionally, the organic components in Kenaf fibres might interact with the cement hydration products, influencing the microstructure and promoting the formation of certain hydrates [62]. On the other hand, the limited impact of PP fibres on the rate of cement hydration can be explained by their inert nature. PP fibres typically do not chemically interact with the cementitious phases and act more as physical reinforcements than active participants in the hydration process [67].

The key points to consider regarding the effects of PP fibres on cement hydration are including water absorption, water-cement ratio, fibre dispersion, surface area and aspect ratio, and fibre content. PP fibres are hydrophobic and do not readily absorb water. This characteristic can affect the availability of water for cement hydration. The presence of PP fibres may result in reduced water content in the cement matrix, potentially slowing down the hydration reaction [68]. The addition of PP fibres may require adjustments to the water-cement ratio to maintain the desired workability. Modifications in the water-cement ratio can indeed influence the hydration process and have the potential to affect the setting time and the development of strength in the cement [69]. Proper dispersion and distribution of PP fibres in the cement matrix are crucial for their effectiveness. Inadequate dispersion can lead to the formation of fibre clusters, which can hinder the hydration process in localized areas and create voids [70]. The surface area and aspect ratio of PP fibres can affect their interaction with cement-based materials. An increased surface area or aspect ratio can enhance the physical connection between the fibres and the cement matrix, potentially leading to alterations in the hydration kinetics [71]. The amount or volume fraction of PP fibres added to cement can impact the hydration rate. Higher fibre content can reduce the availability of water for hydration, leading to delayed or slower hydration [72]. The outcomes of the thermogravimetric analysis (TGA) for the cement-based composite containing 1.5% Kenaf (K-1.5) and 2.0% polypropylene (P-2.0) are depicted in figure 24(a). The differential scanning calorimetry (DSC) curves shown in figure 24(b) offer a precise evaluation of the temperature linked to each decay related to the decomposition of a constituent.

The temperature at which weight loss occurs in TGA analysis can provide indications of specific hydration products and their thermal stability. Indeed, the TGA curve can be delineated into distinct stages, each corresponding to the dehydration of specific cement hydration products. The initial stage, observable in the TGA diagrams, extends up to 105 °C and primarily pertains to the removal of moisture and free water from the cement-based composite [73]. In the temperature range between 105 and 400 °C, a second stage of decline signifies the dehydration of chemically bonded water inherent in the cement hydrates. Subsequently, a third stage of decline, occurring between 400 and 550 °C, is linked to the dehydroxylation of calcium hydroxide (CH). Finally, there is a decline between 600 and 800 °C, attributed to the presence of calcium carbonate originating from the clinker and the carbonation of cement [34]. These observations align with the prior discussion regarding the improvement of the cement hydration process and the increased formation of hydration products as a consequence of incorporating CNT/GNPs and treated natural fibres into the composites. In general, the inclusion of natural fibres in cement-based composites results in an augmented moisture content within the microstructure, thereby potentially accelerating the cement hydration rate. Generally, the water absorption and chemical composition of natural fibres can contribute to increased cement hydration and bonding with the cement matrix in several ways including water retention, capillary action, surface reactivity, alkaline activation,

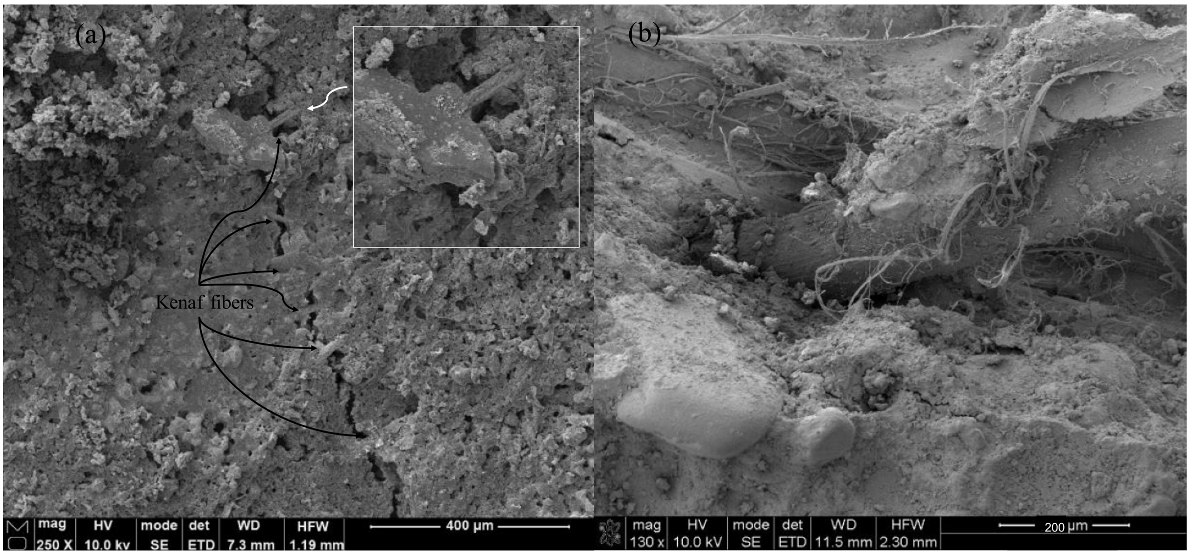

Figure 25. SEM morphology images of the cement-based composite reinforced with fibres: (a) Kenaf fibres, (b) PP fibres.

and microstructural effects. Natural fibres have the ability to absorb and retain water. When incorporated into cement-based composites, these fibres can act as reservoirs, holding water within the material. The retained water provides a continuous source for cement hydration, allowing for a prolonged and sustained hydration process. This sustained hydration promotes the formation of hydration products and facilitates the bonding between the cement matrix and the fibres [43]. Natural fibres possess capillary structures that allow them to absorb and transport water. This capillary action can draw water from the surrounding cement-based matrix, promoting better water distribution within the composite. The improved water distribution facilitates the hydration of cement particles, leading to enhanced cement hydration and bonding [74]. The chemical composition of natural fibres can indeed contribute to improving the adhesion between the fibres and the cement matrix. Some natural fibres, such as sisal or jute, contain lignocellulosic components that are reactive with cement-based materials. These reactive components can chemically interact with the hydration products of cement, forming bonds and improving the overall adhesion between the fibres and the matrix [43]. Cement-based materials exhibit high pH levels owing to the presence of CH formed during the hydration process. The alkaline environment can activate certain natural fibres, causing chemical modifications on their surfaces. These modifications can create additional bonding sites for the cement-based matrix, leading to improved adhesion and interfacial strength [75]. The incorporation of natural fibres can influence the microstructure of cement-based composites. The fibres can help in creating a more porous and interconnected network within the matrix, facilitating the transport of water and ions during the hydration process. Enhanced transport properties can expedite the cement hydration process and facilitate stronger bonding between cement matrix and fibres [76]. Accordingly, the natural fibres might have better interface conditions with the cement matrix leading to proper stress transition to the fibre and bridging the cracks and avoiding their propagation (figure 25(a)). However, PP fibres were extruded due to their weak interface conditions (figure 25(b)).

3.5. Numerical simulations outputs

3.5.1. Numerical verification model. For the purpose of validation, we generated a simulation of the masonry tunnel model as previously established by Atkinson *et al* [77]. This study aimed to assess the viability of employing the innovative TEM (tunnel enlargement machine) method for the rehabilitation of railway tunnels in the United Kingdom. They used 2D and 3D finite element simulations for feasibility of resizing and relining of Whiteball tunnel in the UK. They conducted simulations of masonry tunnels within their 2D numerical models, embedding them within the ground and incorporating two distinct geological formations, namely Otter Sandstone and Budleigh Salterton Pebble. For comprehensive insights into the properties of the ground mass encircling the tunnel, the attributes of the Whiteball tunnel employed for enlargement and rehabilitation, and the specific input parameters utilized in the numerical validation model, I recommend consulting the work by Atkinson *et al* [77], as detailed in their publication. Within the verification numerical model, the ground surrounding the tunnel lining was emulated using Otter Sandstone formations. The dimensions of the numerical verification model were considered equivalent to those of Atkinson *et al* [77] numerical model. For the numerical model validation, the ground mass was defined using an elastic perfectly plastic constitutive model with MC failure criteria, whereas the tunnel lining was represented by a linear elastic constitutive model. Table 8 provides the specific parameters associated with the MC failure criteria for the ground mass and the lining properties of the masonry tunnel. As shown in figure 26, the main output of the 2D numerical analysis is the maximum total displacement around the tunnel for both the Atkinson *et al* [77] model and the numerical verification model. A reasonable agreement is evident between the

Table 8. The parameters of the numerical verification model.

Parameters	Symbol	Unit	Value
	Properties of the ground (Otter Sandstone)		
Density	ρ	Kg m^{-3}	2200
Young's modulus	E	MPa	2500.0
Poisson's ratio	ν	—	0.2
Friction angle	ϕ	Degrees	40.0
Tensile Strength	σ_t	kPa	1.0
Cohesion	C	kPa	100.0
	Properties of the masonry lining (rings of brick)		
Density	ρ	Kg m^{-3}	2500
Young's modulus	E	GPa	3.0
Poisson's ratio	ν	—	0.2
Thickness	t	m	0.6

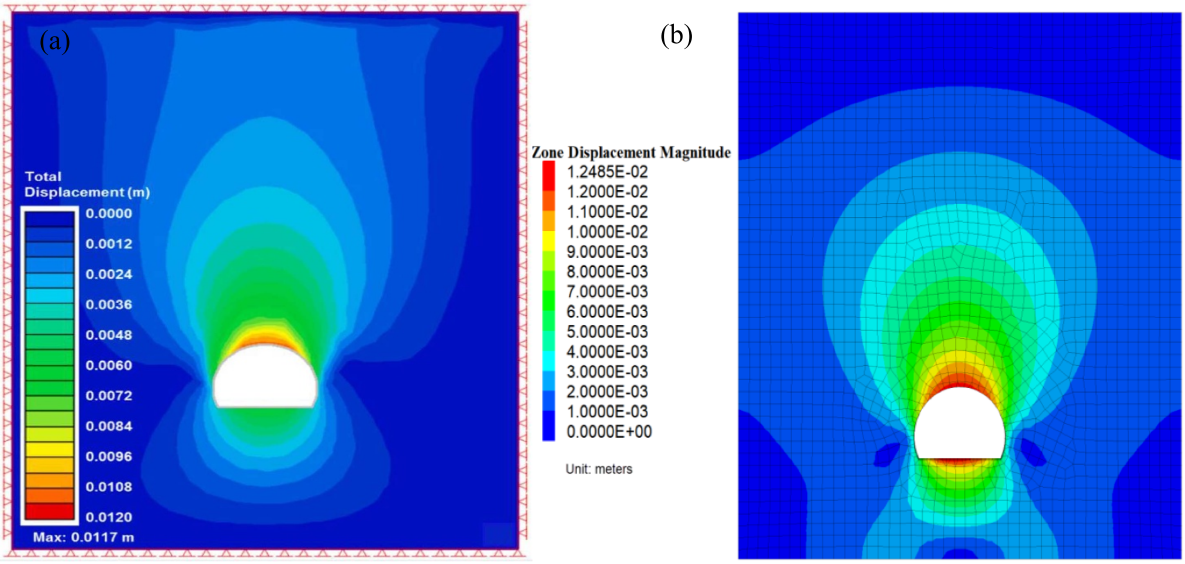

Figure 26. Final displacements after the tunnel enlargement of the preliminary 2D analysis in the Otter Sandstone formation: (a) numerical model of the masonry tunnel conducted by Atkinson *et al* [77] (Reprinted from Atkinson *et al* [77] Copyright 2021, with permission from Elsevier), (b) numerical model for verification.

outcomes of the numerical validation model and the numerical model presented in the work by Atkinson *et al* [77]. In both numerical models, the most significant distribution of total displacement is notably concentrated in the upper region of the tunnel, often referred to as the crown area.

3.5.2. Reference case numerical models. In this section, we provide an extensive discussion of the outcomes derived from the numerical models of the access tunnels situated within the premises of the Iran Mall shopping center. Figure 27 visually represents the contour maps of vertical displacement in the tunnel models under three distinct tunnel shotcrete scenarios: shotcrete without fibres, shotcrete integrated with Kenaf fibres (1.5%), and shotcrete reinforced with PP fibres (2.0%). This analysis delves into the examination of the influence of natural fibres within the context of the most demanding scenario, encompassing considerations related to loading and excavation sequences. In figure 27(a), corresponding to the tunnel case where shotcrete without fibres was employed, the contour map of vertical displacement depicts elevated settlement levels in the tunnel crown, as well as ground surface settlement, and uplift in the invert. In contrast, figures 27(b) and (c), representing the tunnel scenarios with shotcrete containing fibres, exhibit reduced settlement patterns. Specifically, the maximum settlement observed in the tunnel crown for the shotcrete without fibres amounts to 7.42 cm. A comparative analysis of the displacement at the tunnel crown in relation to ground surface settlement reveals that the inclusion of Kenaf and PP fibres results in a reduction of over 50% in both vertical displacements at the tunnel crown and ground surface settlement.

As depicted in figure 28, the contour maps display the vertical increment strain patterns in the tunnel models subjected to

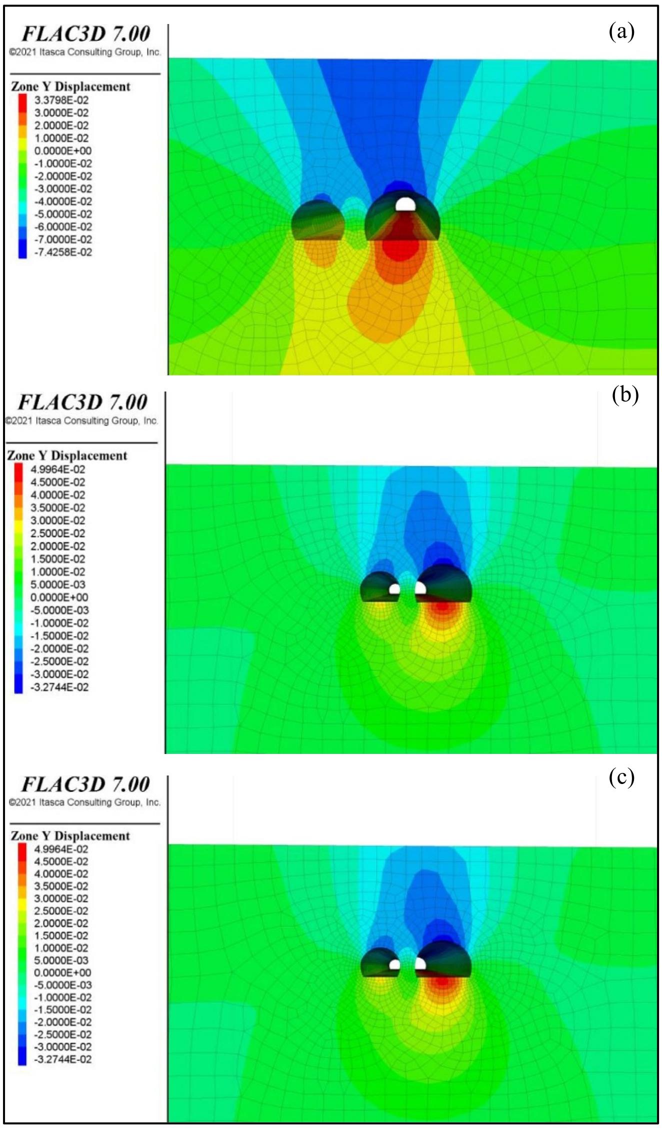

Figure 27. Vertical displacement contours of the tunnel numerical models with different shotcrete types (static loading): (a) without fibres, (b) with the optimum percentage of PP fibres (2.0%), (c) with the optimum percentage of Kenaf fibres (1.5%).

three different tunnel shotcrete conditions: shotcrete without fibres, shotcrete reinforced with Kenaf fibres (at the optimal percentage of 1.5%), and shotcrete enhanced with PP fibres (at the optimal percentage of 2.0%) for static loading scenarios. These contours reveal that the maximum vertical increment strain in the tunnel wall without the use of PP and Kenaf fibres in the shotcrete amounts to approximately 3.2×10^{-4}. Conversely, the tunnel walls with shotcrete incorporating PP and Kenaf fibres experiences a maximum vertical increment strain of around 2.6×10^{-4}. Consequently, employing shotcrete with fibre reinforcement in the twin tunnel wall region led to a 25% reduction in vertical increment strain in the vicinity of the tunnel wall.

It is noteworthy that, particularly in the lower section of the tunnel, the tunnel featuring shotcrete with PP and Kenaf fibres exhibits lower vertical increment strain compared to the tunnel without fibre reinforcement.

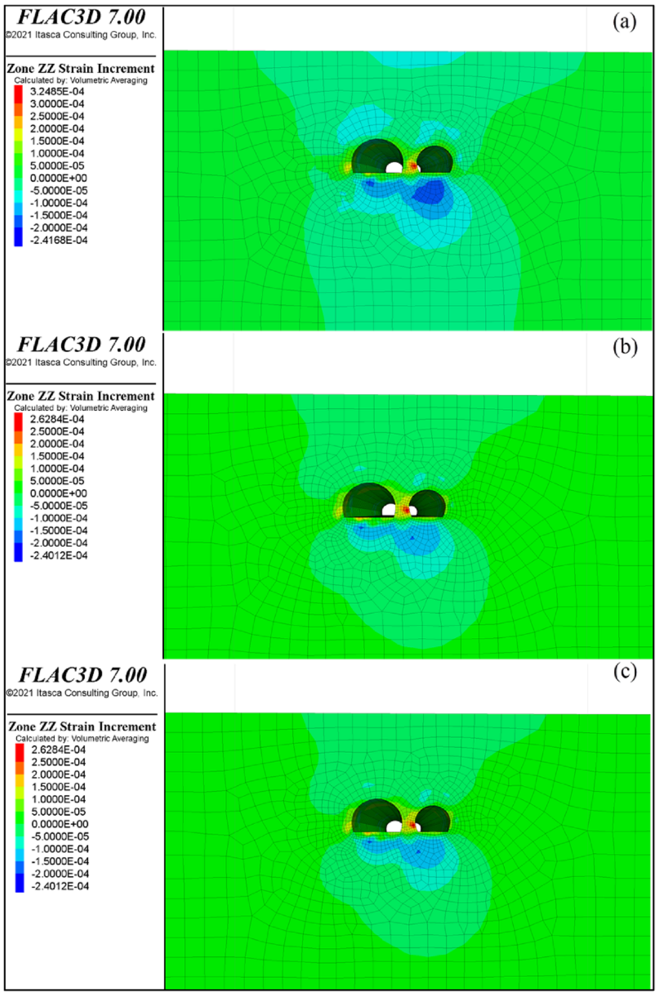

Figure 28. Vertical increment strain contours of the tunnel numerical models with different shotcrete types under static loading: (a) without fibres, (b) with the optimum percentage of PP fibres (2.0%), (c) with the optimum percentage of Kenaf fibres (1.5%).

Figures 29–31, display the vertical displacement of the shotcrete lining in the twin tunnels subjected to harmonic seismic loading (with PGA = 0.02 g). The figures illustrate the scenarios of shotcrete without fibres, shotcrete with Kenaf fibres (at the optimal percentage of 1.5%), and shotcrete with PP fibres (at the optimal percentage of 2.0%) for the invert, crown, and wall of the tunnel shotcrete lining. As shown in figure 29(a), the uplift time history of the tunnel 1 shotcrete lining with Kenaf fibres exhibits fewer fluctuations compared to shotcrete without fibres and shotcrete with PP fibres. The uplift time history of shotcrete with PP fibres also displays less variation than that of shotcrete without fibres. The presence of fibres in the tunnel shotcrete becomes progressively more apparent as the duration of seismic loading increases, resulting in a reduction in the uplift of the tunnel 1 shotcrete invert. At the conclusion of the seismic event, the maximum uplift values are 1.7 mm, 2.1 mm, and 3.1 mm for shotcrete tunnels with Kenaf fibres, shotcrete tunnels with PP fibres, and shotcrete tunnels without fibres, respectively. The diagram clearly shows that the influence of fibres in the shotcrete

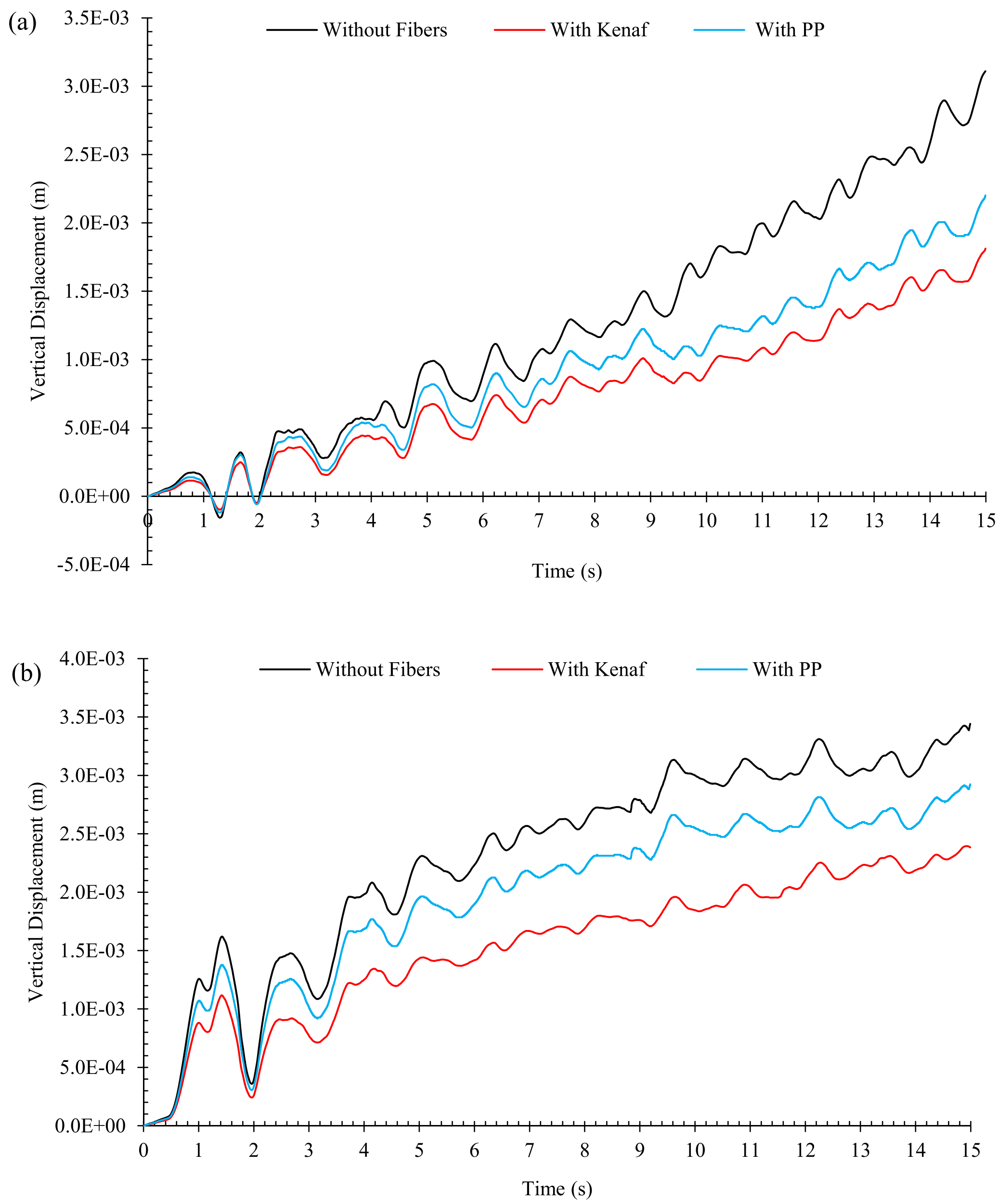

Figure 29. Vertical displacement curves of the tunnel shotcrete invert with different shotcrete types (uplift): (a) Tunnel 1 invert, (b) Tunnel 2 invert.

lining of the tunnel becomes noticeable after two seconds of seismic loading and reaches its maximum value at the end of the seismic event. Figure 29(b) illustrates the uplift time history of tunnel 2 shotcrete lining with Kenaf fibres, which displays fewer variations compared to shotcrete without fibres and shotcrete with PP fibres. At the end of the seismic event, the maximum uplift values for the different shotcrete scenarios are as follows: 2.3 mm for shotcrete with Kenaf fibres, 2.8 mm for shotcrete with PP fibres, and 3.4 mm for shotcrete without fibres. Both figures 29(a) and (b), emphasize the impact of fibres on the performance of tunnel shotcrete under seismic loading. Notably, the uplift of the tunnel invert in both tunnels No. 1 and No. 2 has been reduced by 45% and 32%, respectively, through the utilization of shotcrete with Kenaf fibres.

Figures 30 and 31, provide visual representations of how the inclusion of Kenaf and PP fibres in the tunnel shotcrete contributes to the reduction of displacements in the tunnel wall and crown. Figure 30(a) demonstrates that the inclusion of shotcrete with Kenaf fibres in tunnel 1 results in a 36% reduction in the displacement of the tunnel crown during seismic loading. Likewise, figure 30(b) depicts that shotcrete with Kenaf fibres in tunnel 2 diminishes the displacement of the tunnel crown by 33% under seismic loading. Figure 31(a), illustrates that the incorporation of shotcrete with Kenaf fibres

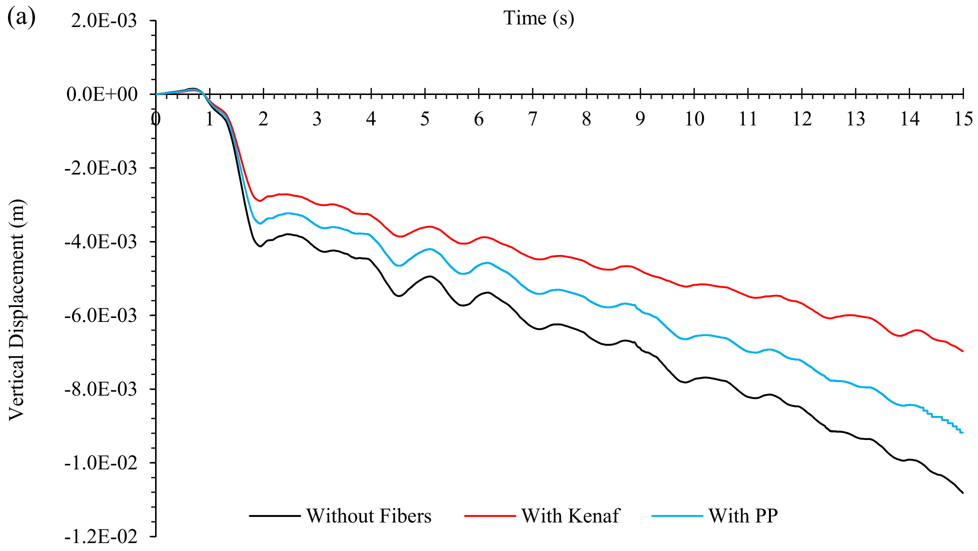

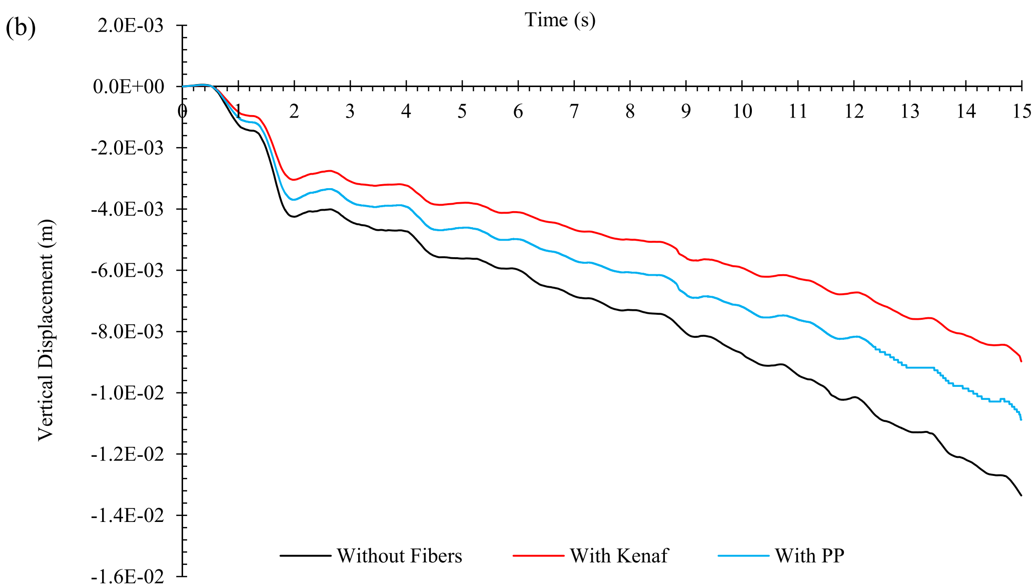

Figure 30. Vertical displacement curves of the tunnel shotcrete crown with different shotcrete types (settlement): (a) Tunnel 1 crown, (b) Tunnel 2 crown.

in tunnel 1 results in a 43% reduction in the displacement of the tunnel wall under seismic loading. Similarly, figure 31(b), demonstrates that shotcrete with Kenaf fibres in tunnel 2 decreases the displacement of the tunnel wall by 39% under seismic loading. Conclusively, as evidenced by figures 29–31, it is apparent that shotcrete with Kenaf fibres exhibits superior performance compared to shotcrete with PP fibres under seismic loading conditions. Moreover, both shotcrete options featuring Kenaf and PP fibres outperform shotcrete lining without any fibres.

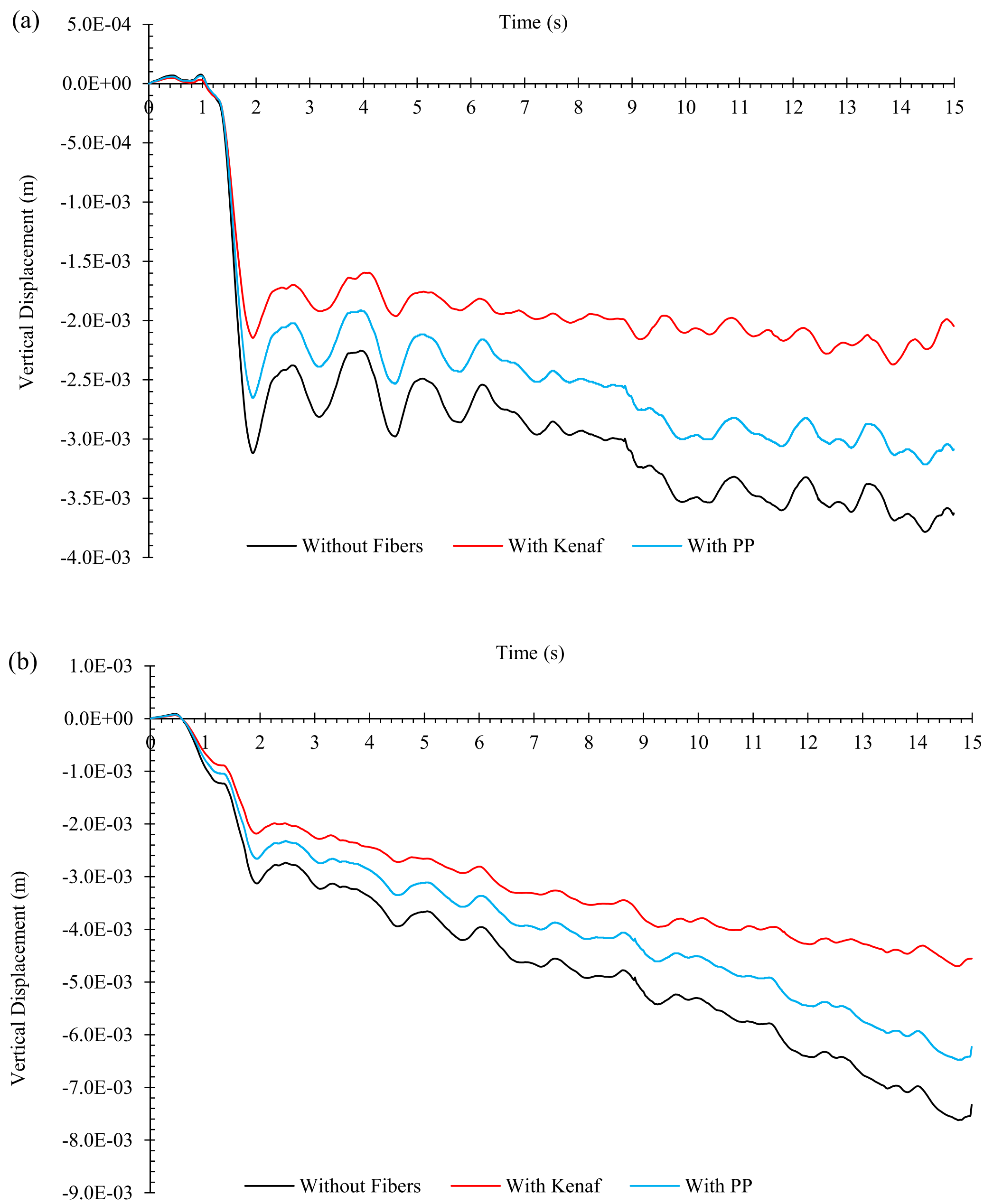

Figure 31. Vertical displacement curves of the tunnel shotcrete wall with different shotcrete types (settlement): (a) Tunnel 1 left wall, (b) Tunnel 2 right wall.

4. Conclusions

In this research, a sustainable multifunctional cement-based composite was developed for shotcrete application using different percentages of Kenaf fibres and hybrid CNT/GNPs. The physical, sensing, and heating potentials of this green shotcrete mixture were investigated using several tests and compared with the mixture containing a common synthesis fibre of PP in different percentages. Furthermore, a detailed 3D nonlinear finite difference model of an urban line tunnel including all components was developed using the optimum experimental outcomes and validated. The performances of this green shotcrete mixture as the lining of the inner shell of the tunnel were assessed comparatively using this 3D numerical model under static and seismic loading, and the following conclusions were drawn:

- Increasing Kenaf and PP fibre concentrations in concrete composites raised DC resistivity proportionally, disrupting conductive pathways in hybrid CNT/GNP-reinforced cementitious composites. The insulating properties of fibres led to a rise in electrical resistivity. Under cyclic compressive loading, negative FCR values indicated reduced resistivity during compression, with PP fibres showing lower absolute FCR values than Kenaf. The incorporation of fibres impacted the stability of joule heating, influencing electrical resistivity in the CNT/GNP cement composite.

- Elevated Kenaf and PP fibre concentrations in conductive cement composites resulted in reduced peak temperature and heating rate during joule heating, driven by insulating fibre properties, disrupting the CNT/GNP conductive network.
- A general reduction in compression strength was observed in the composites when Kenaf and PP fibres were incorporated. The incorporation of optimum percentages of Kenaf (1.5%) and PP fibres (2.0%) into the concrete, reduced the compressive strength by around 9.0 and 16% respectively compared to the plain sample.
- The maximum compression elastic module was obtained for the specimens K-1.5 and PP-2 which were relatively equal to the plain sample. While the addition of 1.5 and 2.0% of the Kenaf and PP fibres improved the rapture modulus of the composite by approximately 45 and 25% respectively.
- The analysis using DIC demonstrated that the Kenaf fibres exhibited notable potential in reducing crack opening and enhancing crack propagation compared to the PP fibres in the cement-based composite.
- In comparison with plain concrete, the composites reinforced with 1.5 and 2.0% of Kenaf and PP fibres, showed an improvement in flexural strength by approximately 83 and 28% respectively.
- Microstructural analysis revealed a minimal decrease in the hardened density of the specimens that were reinforced with the optimal proportions of Kenaf and PP fibres. This reduction resulted in a decrease in ultrasonic pulse velocity.
- TGA and XRD analyses demonstrated the beneficial impact of Kenaf fibres in terms of accelerating the cement hydration rate.
- A 3DNLFD numerical model for an urban line tunnel including all components and green shotcrete was developed. Results of the comparative static analysis indicated the higher performance of the Kenaf fibre (optimum percentage, 1.5%) and the PP fibres (optimum percentage, 2.0%) compared to shotcrete without fibres in reducing the settlement of the tunnel crown, the settlement of the ground surface, the tunnel invert uplift, and vertical increment strain (vertical total strain).
- A time history of displacement and response for shotcrete linings in twin tunnels exposed to seismic harmonic loading reveals that both Kenaf and PP fibres exert a substantial reinforcing effect on shotcrete, leading to a notable reduction in displacement across the invert, crown, and walls of the shotcrete lining. Notably, the performance of shotcrete with Kenaf fibres outpaces that of shotcrete with PP fibres, particularly when subjected to seismic loading. However, under static loading conditions resulting from in-situ loads, both Kenaf and PP fibre-reinforced shotcrete respond in a comparable manner.

Overall, the results of this study underscore the considerable potential of natural fibres in the development of multifunctional sustainable, cost-effective, and reliable cement-based composites for tunnel shotcrete applications.

Data availability statement

All data that support the findings of this study are included within the article (and any supplementary files).

Acknowledgments

The authors wish to express their gratitude to the Auckland University of Technology (AUT), New Zealand, for their collaboration in confirming the modelling aspects of this study using the academic license of the FLAC^{3D} Version 7.00 software provided by the Itasca Consulting Group, Minneapolis, USA.

The authors acknowledge the support of the European Commission-Shift2Rail Program under the Project 'IN2TRACK3, H2020-S2RJU-CFM-2020-S2R-CFMIP3-01-2020'. The authors acknowledge also the support provided by FCT/MCTES through national funds (PIDDAC), under the R&D Unit Institute for Sustainability and Innovation in Structural Engineering (ISISE), under reference UIDB/04029/2020, under Project UIDB/QUI/00686/2020 of CQ, and also under the Associate Laboratory Advanced Production and Intelligent Systems ARISE under reference LA/P/0112/2020, as well as under the R&D Unit Centre for Textile Science and Technology (2C2T) under the Project UIDB/00686/2021.

The first author acknowledges also the support provided by the FCT/PhD individual fellowship with reference of '2021.07596.BD.'

Conflicts of interest

The authors have no conflicts of interest to declare.

Ethics statement

This study does not contain any studies involving human or animal participants.

ORCID iDs

Mohammadmahdi Abedi https://orcid.org/0000-0002-2920-9284
Federico Gulisano https://orcid.org/0000-0002-1595-5665
Baoguo Han https://orcid.org/0000-0002-7081-3221
Raul Fangueiro https://orcid.org/0000-0003-3303-6563
António Gomes Correia https://orcid.org/0000-0002-0103-2579

References

[1] Abedi M, Correia A G and Fangueiro R 2021 Geotechnical and piezoresistivity properties of sustainable cementitious stabilized sand reinforced with recycled fibres *Transp. Eng.* **6** 100096

[2] Williams G I and Wool R P 2000 Composites from natural fibers and soy oil resins *Appl. Compos. Mater.* **7** 421–32
[3] García M, Garmendia I and García J 2008 Influence of natural fiber type in eco-composites *J. Appl. Polym. Sci.* **107** 2994–3004
[4] Vitrone F, Ramos D, Ferrando F and Salvadó J 2021 Binderless fiberboards for sustainable construction. Materials, production methods and applications *J. Build. Eng.* **44** 102625
[5] Abedi M, Fangueiro R, Correia A G and Shayanfar J 2023 Smart geosynthetics and prospects for civil infrastructure monitoring: a comprehensive and critical review *Sustainability* **15** 9258
[6] Abedi M, Shayanfar J and Al-Jabri K 2023 Damage assessment via machine learning approaches: a systematic review *Asian J. Civ. Eng.* **24** 1–30
[7] Roshan M J, Abedi M, Correia A G, Raul F and Mendes P M 2023 A multifunctional cementitious composite for pavement subgrade *Materials* **17** 621
[8] Zhou Y, Wang X, Sui L, Xing F, Wu Y and Chen C 2018 Flexural performance of FRP-plated RC beams using H-type end anchorage *Compos. Struct.* **206** 11–21
[9] Bakis C E, Bank L C, Brown V, Cosenza E, Davalos J, Lesko J, Machida A, Rizkalla S H and Triantafillou T C 2002 Fiber-reinforced polymer composites for construction—State-of-the-art review *J. Compos. Constr.* **6** 73–87
[10] Chen C, Wang X, Sui L, Xing F, Chen X and Zhou Y 2019 Influence of FRP thickness and confining effect on flexural performance of HB-strengthened RC beams *Composites* B **161** 55–67
[11] Hassanpour M, Shafigh P and Mahmud H B 2012 Lightweight aggregate concrete fiber reinforcement–A review *Constr. Build. Mater.* **37** 452–61
[12] Song H, Liu J, He K and Ahmad W 2021 A comprehensive overview of jute fiber reinforced cementitious composites *Case Stud. Constr. Mater.* **15** e00724
[13] Abedi M, Fangueiro R and Correia A G 2021 A review of intrinsic self-sensing cementitious composites and prospects for their application in transport infrastructures *Constr. Build. Mater.* **310** 125139
[14] Arjomand M, Abedi M, Gharib M and Damghani M 2019 An experimental study on geogrid with geotextile effects aimed to improve clayey soil *Int. J. Eng.* **32** 685–92
[15] AlShuhail K, Aldawoud A, Syarif J and Abdoun I A 2021 Enhancing the performance of compressed soil bricks with natural additives: wood chips and date palm fibers *Constr. Build. Mater.* **295** 123611
[16] Dos Santos G Z B, de Oliveira D P, de Almeida Melo Filho J and da Silva N M 2021 Sustainable geopolymer composite reinforced with sisal fiber: durability to wetting and drying cycles *J. Build. Eng.* **43** 102568
[17] Oskouei A V, Afzali M and Madadipour M 2017 Experimental investigation on mud bricks reinforced with natural additives under compressive and tensile tests *Constr. Build. Mater.* **142** 137–47
[18] Mostafa M and Uddin N 2016 Experimental analysis of Compressed Earth Block (CEB) with banana fibers resisting flexural and compression forces *Case Stud. Constr. Mater.* **5** 53–63
[19] Al-Azad N, Mojutan E C and Shah M K M 2021 A mini review on natural fiber honeycomb (NFH) sandwiched structure composite: flexural perfomance perspective *J. Mater. Sci. Chem. Eng.* **9** 1–10
[20] Singh C P, Patel R V, Hasan M F, Yadav A, Kumar V and Kumar A 2021 Fabrication and evaluation of physical and mechanical properties of jute and coconut coir reinforced polymer matrix composite *Mater. Today Proc.* **38**: 2572–7
[21] Lertwattanaruk P and Suntijitto A 2015 Properties of natural fiber cement materials containing coconut coir and oil palm fibers for residential building applications *Constr. Build. Mater.* **94** 664–9
[22] Duong N T, Satomi T and Takahashi H (eds) 2020 Study on the compressive and tensile strength behaviors of corn Husk fiber–cement stabilized soil *Int. Conf. on Green Technology and Sustainable Development* (Springer)
[23] Rathod R S B and Reddy B V 2021 Strength and stress–strain characteristics of fibre reinforced cement stabilised rammed earth *Mater. Struct.* **54** 1–13
[24] Thanushan K, Yogananth Y, Sangeeth P, Coonghe J G and Sathiparan N 2021 Strength and durability characteristics of coconut fibre reinforced earth cement blocks *J. Nat. Fibers* **18** 773–88
[25] Baghban M H and Mahjoub R 2020 Natural kenaf fiber and LC3 binder for sustainable fiber-reinforced cementitious composite: a review *Appl. Sci.* **10** 357
[26] Ogunbode B E, Nyakuma B B, Lawal T A, Yatim J M, Abdul A and Ayoosu M I 2021 Morphological, microstructure, tensile and water-sorption characteristics of surface modified kenaf fibre for sustainable biocomposite reinforcement *J. Nat. Fibers* **19** 1–12
[27] Parashar S and Chawla V 2021 Evaluation of fiber volume fraction of kenaf-coir-epoxy based green composite by finite element analysis *Mater. Today Proc.* **50** 1265–74
[28] Banthia N 2019 *Advances in Sprayed Concrete (Shotcrete). Developments in the Formulation and Reinforcement of Concrete* (Elsevier) pp 289–306
[29] Galan I, Baldermann A, Kusterle W, Dietzel M and Mittermayr F 2019 Durability of shotcrete for underground support–Review and update *Constr. Build. Mater.* **202** 465–93
[30] Bernard E S 2020 *Shotcrete: Engineering Developments* (CRC Press)
[31] Liu G, Cheng W and Chen L 2017 Investigating and optimizing the mix proportion of pumping wet-mix shotcrete with polypropylene fiber *Constr. Build. Mater.* **150** 14–23
[32] Othman H, Sabrah T and Marzouk H 2019 Conceptual design of ultra-high performance fiber reinforced concrete nuclear waste container *Nucl. Eng. Technol.* **51** 588–99
[33] Abedi M, Kiran Sanivada U, Ali Mirian S, Hassanshahi O, Al-Jabri K, Gomes Correia A, Lourenço P B and Fangueiro R 2023 A self-sensing and self-heating planar braided composite for smart civil infrastructures reinforcement *Constr. Build. Mater.* **387** 131617
[34] Abedi M, Roshan M J, Gulisano F, Shayanfar J, Adresi M, Fangueiro R and Correia A G 2024 An advanced cement-based geocomposite with autonomous sensing and heating capabilities for enhanced intelligent transportation infrastructure *Constr. Build. Mater.* **411** 134577
[35] Guo Y, Wang D, Ashour A, Ding S and Han B 2023 Self-sensing ultra-high performance concrete: a review *Meas. Sci. Technol.* **35** 032003
[36] Abedi M, Fangueiro R and Correia A G 2021 Effects of multiscale carbon-based conductive fillers on the performances of a self-sensing cementitious geocomposite *J. Build. Eng.* **43** 103171
[37] Kang Z, Aslani F and Han B 2024 Prediction of mechanical and electrical properties of carbon fibre-reinforced self-sensing cementitious composites *Case Stud. Constr. Mater.* **20** e02716
[38] Sun T, Wang X, Maimaitituersun N, Dong S, Li L and Han B 2024 Synergistic effects of steel fibers and steel wires on uniaxial tensile mechanical and self-sensing properties of UHPC *Constr. Build. Mater.* **416** 134991

[39] Qin H, Ding S, Qiu L and Han B 2023 Electrical properties of ultra-high-performance concrete with various reinforcing fibers *Meas. Sci. Technol.* **35** 035601

[40] Abedi M, Fangueiro R and Correia A G 2021 Innovative self-sensing fiber-reinforced cemented sand with hybrid CNT/GNP *Smart Mater. Struct.* **30** 105034

[41] Abedi M, Fangueiro R and Correia A G 2022 Effects of electrodes layout and filler scale on percolation threshold and piezoresistivity performances of a cementitious-based geocomposite *Nanomaterials* **12** 1734

[42] Abedi M, Hassanshahi O, Barros J A, Correia A G and Fangueiro R 2022 Three-dimensional braided composites as innovative smart structural reinforcements *Compos. Struct.* **297** 115912

[43] Abedi M, Hassanshahi O, Rashiddel A, Ashtari H, Seddik Meddah M, Dias D, Arjomand M A and Keong Choong K 2023 A sustainable cementitious composite reinforced with natural fibers: an experimental and numerical study *Constr. Build. Mater.* **378** 131093

[44] Qiu L, Ding S, Wang D and Han B 2023 Self-sensing GFRP-reinforced concrete beams containing carbon nanotube-nano carbon black composite fillers *Meas. Sci. Technol.* **34** 084003

[45] Celik D N, Yıldırım G, Al-Dahawi A, Ulugöl H, Han B and Şahmaran M 2021 Self-monitoring of flexural fatigue damage in large-scale steel-reinforced cementitious composite beams *Cem. Concr. Compos.* **123** 104183

[46] Ding S, Dong S, Wang X, Ding S, Han B and Ou J 2023 Self-heating ultra-high performance concrete with stainless steel wires for active deicing and snow-melting of transportation infrastructures *Cem. Concr. Compos.* **138** 105005

[47] Abedi M, Fangueiro R, Camões A and Correia A G 2020 Evaluation of CNT/GNP's synergic effects on the Mechanical, Microstructural, and durability properties of a cementitious composite by the novel dispersion method *Constr. Build. Mater.* **260** 120486

[48] Abedi M, Fangueiro R and Correia A G 2020 An effective method for hybrid CNT/GNP dispersion and its effects on the mechanical, microstructural, thermal, and electrical properties of multifunctional cementitious composites *J. Nanomater.* **2020** 6749150

[49] Abedi M, Fangueiro R and Gomes Correia A 2020 Ultra-sensitive affordable cementitious composite with high mechanical and microstructural performances by hybrid CNT/GNP *Materials* **13** 3484

[50] Gholampour A and Ozbakkaloglu T 2020 A review of natural fiber composites: properties, modification and processing techniques, characterization, applications *J. Mater. Sci.* **55** 829–92

[51] Bentur A and Mindess S 2006 *Fibre Reinforced Cementitious Composites* (CRC Press)

[52] Lilargem Rocha D, Tambara Júnior L U D, Marvila M T, Pereira E C, Souza D and de Azevedo A R G 2022 A review of the use of natural fibers in cement composites: concepts, applications and Brazilian history *Polymers* **14** 2043

[53] Ozerkan N G, Ahsan B, Mansour S and Iyengar S R 2013 Mechanical performance and durability of treated palm fiber reinforced mortars *Int. J. Sustain. Built. Environ.* **2** 131–42

[54] Snoeck D, Smetryns P-A and De Belie N 2015 Improved multiple cracking and autogenous healing in cementitious materials by means of chemically-treated natural fibres *Biosyst. Eng.* **139** 87–99

[55] Hamidon M H, Sultan M T, Ariffin A H and Shah A U 2019 Effects of fibre treatment on mechanical properties of kenaf fibre reinforced composites: a review *J. Mater. Res. Technol.* **8** 3327–37

[56] Itasca Consulting Group 2002 *FLAC3D : Fast Lagrangian Analysis of Continua in 3 Dimensions* (Itasca Consulting Group, Minneapolis, Minn)

[57] Rashiddel A, Hajihassani M, Kharghani M, Valizadeh H, Rahmannejad R and Dias D 2022 Numerical analysis of segmental tunnel linings-Use of the beam-spring and solid-interface methods *Geomech. Eng.* **29** 471–86

[58] Rashiddel A, Kharghani M, Dias D and Hajihassani M 2020 Numerical study of the segmental tunnel lining behavior under a surface explosion–Impact of the longitudinal joints shape *Comput. Geotech.* **128** 103822

[59] Ramesh A, Rashiddel A, Hajihassani M, Dias D and Kiani M 2023 Interaction of segmental tunnel linings and dip-slip Faults—Tabriz subway tunnels *Appl. Sci.* **13** 7866

[60] Srivastav A, Satyam N and Rajan K 2022 Seismic vulnerability assessment of steel fiber reinforced shotcrete lined (SFRS) tunnel: a himalayan case study *J. Geol. Soc. India* **98** 185–92

[61] Rashiddel A, Abedi M, Dias D and Ramesh A 2024 Seismic analysis of segmental shallow tunnels adjacent to building foundations under soil liquefaction and its mitigation *Soil Dyn. Earthq. Eng.* **178** 108479

[62] Onuaguluchi O and Banthia N 2016 Plant-based natural fibre reinforced cement composites: a review *Cem. Concr. Compos.* **68** 96–108

[63] Saba N, Paridah M and Jawaid M 2015 Mechanical properties of kenaf fibre reinforced polymer composite: a review *Constr. Build. Mater.* **76** 87–96

[64] Zhou C, Cai L, Chen Z and Li J 2020 Effect of kenaf fiber on mechanical properties of high-strength cement composites *Constr. Build. Mater.* **263** 121007

[65] Abedi M, Fangueiro R and Correia A G 2021 Development of a novel multifunctional cementitious-based geocomposite by the contribution of CNT and GNP *Nanomaterials* **11** 961

[66] Li Z, Corr D J, Han B and Shah S P 2020 Investigating the effect of carbon nanotube on early age hydration of cementitious composites with isothermal calorimetry and Fourier transform infrared spectroscopy *Cem. Concr. Compos.* **107** 103513

[67] Bouziani T, Benmounah A, Makhloufi Z, Bédérina M and Queneudec T'kint M 2014 Properties of flowable sand concretes reinforced by polypropylene fibers *J. Adhes. Sci. Technol.* **28** 1823–34

[68] Agustini N K A, Triwiyono A, Sulistyo D and Suyitno S 2021 Mechanical properties and thermal conductivity of fly ash-based geopolymer foams with polypropylene fibers *Appl. Sci.* **11** 4886

[69] Abid S R, Shamkhi M S, Mahdi N S and Daek Y H 2018 Hydro-abrasive resistance of engineered cementitious composites with PP and PVA fibers *Constr. Build. Mater.* **187** 168–77

[70] Amuchi M, Abtahi S M, Koosha B, Hejazi S M and Sheikhzeinoddin H 2015 Reinforcement of steel-slag asphalt concrete using polypropylene fibers *J. Ind. Text.* **44** 526–41

[71] Tastani S P, Konsta-Gdoutos M S, Pantazopoulou S J and Balopoulos V 2016 The effect of carbon nanotubes and polypropylene fibers on bond of reinforcing bars in strain resilient cementitious composites *Front. Struct. Civ. Eng.* **10** 214–23

[72] Patti A, Nele L, Zarrelli M, Graziosi L and Acierno D 2021 A comparative analysis on the processing aspects of basalt and glass fibers reinforced composites *Fibers Polym.* **22** 1449–59

[73] Meddah M S, Al Owaisi M, Abedi M and Hago A W 2023 Mortar and concrete with lime-rich calcined clay pozzolana: a sustainable approach to enhancing performances and reducing carbon footprint *Constr. Build. Mater.* **393** 132098

[74] Camargo M M, Adefrs Taye E, Roether J A, Tilahun Redda D and Boccaccini A R 2020 A review on natural fiber-reinforced geopolymer and cement-based composites *Materials* **13** 4603

[75] Benmokrane B, Ali A H, Mohamed H M, Robert M and ElSafty A 2016 Durability performance and service life of CFCC tendons exposed to elevated temperature and alkaline environment *J. Compos. Constr.* **20** 04015043

[76] Bordoloi S, Sekharan S and Garg A 2017 A review of physio-biochemical properties of natural fibers and their application in soil reinforcement *Adv. Civ. Eng. Mater.* **6** 323–59

[77] Atkinson C, Paraskevopoulou C and Miller R 2021 Investigating the rehabilitation methods of Victorian masonry tunnels in the UK *Tunn. Undergr. Space Technol.* **108** 103696